

AD-A036 900

AUBURN UNIV ALA DEPT OF AEROSPACE ENGINEERING  
AERODYNAMIC INTERFERENCE OF TWO AXISYMMETRIC STORES AT LOW SUPE--ETC(U)  
OCT 76 J E BURKHALTER, F W MARTIN

F08635-76-C-0079

AFATL-TR-76-116

NL

UNCLASSIFIED

| OF |

AD  
A036900

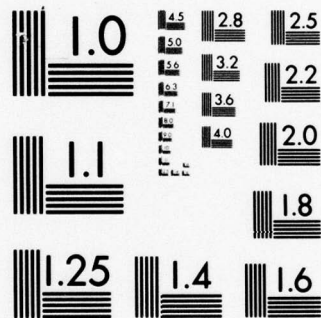
AD  
A036900



END

DATE  
FILMED

4-77



MICROCOPY RESOLUTION TEST CHART  
NATIONAL BUREAU OF STANDARDS-1963-A

AD A036900

AFATL-TR-76-116

**AERODYNAMIC INTERFERENCE  
OF TWO AXISYMMETRIC STORES  
AT LOW SUPERSONIC SPEEDS**

DEPARTMENT OF AEROSPACE ENGINEERING  
AUBURN UNIVERSITY  
AUBURN, ALABAMA 36830

OCTOBER 1976

FINAL REPORT: SEPTEMBER 1975 - SEPTEMBER 1976

**COPY AVAILABLE TO DDC DOES NOT  
PERMIT FULLY LEGIBLE PRODUCTION**

Approved for public release; distribution unlimited.

**AIR FORCE ARMAMENT LABORATORY**

AIR FORCE SYSTEMS COMMAND • UNITED STATES AIR FORCE

**EGLIN AIR FORCE BASE, FLORIDA**



UNCLASSIFIED

SECURITY CLASSIFICATION OF THIS PAGE (When Data Entered)

19 REPORT DOCUMENTATION PAGE		READ INSTRUCTIONS BEFORE COMPLETING FORM	
1. REPORT NUMBER	2. GOVT ACCESSION NO.	3. RECIPIENT'S CATALOG NUMBER	
AFATL-TR-76-116			
4. TITLE (and Subtitle)		5. TYPE OF REPORT & PERIOD COVERED	
AERODYNAMIC INTERFERENCE OF TWO AXISYMMETRIC STORES AT LOW SUPERSONIC SPEEDS.		Final Report: Sep 1975 - Sep 1976	
6. AUTHOR(S)		7. PERFORMING ORG. REPORT NUMBER	
John E. Burkhalter Fred W. Martin		12	
9. PERFORMING ORGANIZATION NAME AND ADDRESS		8. CONTRACT OR GRANT NUMBER(S)	
Department of Aerospace Engineering Auburn University Auburn, Alabama 36830		F08635-76-C-0079 mu	
11. CONTROLLING OFFICE NAME AND ADDRESS		10. PROGRAM ELEMENT, PROJECT, TASK AREA & WORK UNIT NUMBERS	
Air Force Armament Laboratory Armament Development and Test Center Eglin Air Force Base, Florida 32542		Project No. 2567 Task No. 02 Work Unit No. 005	
14. MONITORING AGENCY NAME & ADDRESS (if different from Controlling Office)		12. REPORT DATE	
55p. 16 2567		October 1976	
15. SECURITY CLASS. (of this report)		13. NUMBER OF PAGES	
UNCLASSIFIED		65	
16. DISTRIBUTION STATEMENT (of this Report)		15a. DECLASSIFICATION/DOWNGRADING SCHEDULE	
Approved for public release; distribution unlimited.			
17. DISTRIBUTION STATEMENT (of the abstract entered in Block 20, if different from Report)			
17 02			
18. SUPPLEMENTARY NOTES			
Available in DDC			
19. KEY WORDS (Continue on reverse side if necessary and identify by block number)			
Aerodynamic Interference Multiple Bodies of Revolution Mutual Interference Supersonic Flow			
20. ABSTRACT (Continue on reverse side if necessary and identify by block number)			
A method for determining the basic pressure distribution on an axisymmetric body in supersonic flow has been evaluated. Supersonic line sources with linearly varying strengths placed along the centerline of the body were used to generate the body shape. The results of these theoretical computations for an isolated body agreed very well with experimental data. Two approaches were investigated to determine the pressure distribution on two bodies interfering with each other. In the first approach supersonic point			

DD FORM 1 JAN 73 1473

EDITION OF 1 NOV 65 IS OBSOLETE

UNCLASSIFIED

SECURITY CLASSIFICATION OF THIS PAGE (When Data Entered)

401926



UNCLASSIFIED

SECURITY CLASSIFICATION OF THIS PAGE(When Data Entered)

20. ABSTRACT (Concluded)

sources were placed along an image line, as determined by subsonic theory, and along the body centerline. The strengths of these point sources were determined so that body boundary conditions were met on top and bottom of each interfering body. Computational problems were encountered with this technique resulting from the nature of induced velocities from a supersonic point source and the approach was finally abandoned. The second interference approach utilized linearly varying line sources placed along an image line and along the body centerline. The location of the image line is solely a function of the  $\Delta x$  interval chosen for the problem. As before, body boundary conditions were met on top and on bottom of each interfering body. The results of these computations appear realistic for thin bodies. Interference computations for the M117 store were successful on the nose and center section of the body at low supersonic Mach numbers, but no results were obtained on the aft tail section because of computational problems associated with expansion of supersonic flow around the sharp aft shoulder.

*Delta-4*

UNCLASSIFIED

SECURITY CLASSIFICATION OF THIS PAGE(When Data Entered)


## PREFACE

The work described in this report was done during the period from September 1975 to September 1976 by the Department of Aerospace Engineering, Auburn University, Auburn, Alabama 36830, under Contract Number F08635-76-C-0079 with the Air Force Armament Laboratory, Armament Development and Test Center, Eglin Air Force Base, Florida. The program managers were Lieutenant Norman O. Speakman and Captain R. A. Grow (DLJC). This work was part of the total effort under this contract.

This report has been reviewed by the Information Office (OI) and is releasable to the National Technical Information Service (NTIS). At NTIS, it will be available to the general public, including foreign nations.

This technical report has been reviewed and is approved for publication.

FOR THE COMMANDER

  
WILLIAM F. BROCKMAN, Colonel, USAF  
Chief, Munitions Division

ACCESSION FOR	
NTIS	White Section <input checked="" type="checkbox"/>
DDC	Buff Section <input type="checkbox"/>
UNANNOUNCED	
JUSTIFICATION	
BY DISTRIBUTION/AVAILABILITY CODES	
DMC	APRIL 28/76 SPECIAL
A	

# TABLE OF CONTENTS

Section	Title	Page
I	INTRODUCTION . . . . .	1
II	ISOLATED BODY SOLUTION . . . . .	2
	1. Theory . . . . .	2
	2. Results for Body Shape A4V1P . . . . .	7
	3. Results for the M117 Body Shape . . . . .	10
III	TWO BODY SOLUTION. . . . .	15
	1. Point Source Image Solution . . . . .	15
	Geometry . . . . .	15
	Computational procedure. . . . .	17
	Results of Point Source Solution . . . . .	17
	2. Line Source Image Solution . . . . .	18
	3. Results for Body Shape A4V1P . . . . .	23
	4. Results for the M117 Body Shape . . . . .	29
	5. Surface Velocities on the M117 . . . . .	33
IV	CONCLUSIONS AND RECOMMENDATIONS. . . . .	36
	REFERENCES . . . . .	38
Appendix		
A	COMPUTER PROGRAM DOCUMENTATION . . . . .	39



# LIST OF FIGURES

Figure	Title	Page
1	Line Source in Supersonic Flow . . . . .	3
2	Schematic of the Nose of a Body in Supersonic Flow . . .	4
3	Comparison of Theoretical and Experimental Pressure Distribution for the A4VIP Missile at $\alpha=0.0$ and $M=1.87$ .	8
4	Comparison of Theoretical and Experimental Pressure Distribution for the A4VIP Missile at $\alpha=0.0$ and $M=1.56$ .	9
5	Nose and Centerbody Section of the M117 Store. . . . .	10
6	Comparison of Theoretical and Experimental Pressure Distribution for the M117 Store at $\alpha=0.0$ and $M=1.1$ . . .	11
7	Theoretical Pressure Distribution for the M117 Store at $\alpha=0.0$ and $M=1.3$ . . . . .	12
8	Theoretical Pressure Distribution for the M117 Store at $\alpha=0.0$ and $M=1.5$ . . . . .	13
9	Schematic of Two-Body Interference Geometry Using Point Sources. . . . .	16
10	Schematic of Two-Body Interference Geometry Using Line Sources . . . . .	19
11	Schematic of the Nose Section of an Interfering Body . .	20
12	Interference Axial Pressure Distribution for the A4VIP, $M=1.30$ . . . . .	24
13	Interference Axial Pressure Distribution for the A4VIP, $M=1.56$ . . . . .	25
14	Interference Axial Pressure Distribution for the A4VIP, $M=1.87$ , 60 Line Sources. . . . .	26
15	Interference Axial Pressure Distribution for the A4VIP, $M=1.87$ , 120 Line Sources . . . . .	27



# LIST OF FIGURES (CONCLUDED)

Figure	Title	Page
16	Interference Axial Pressure Distribution for the A4V1P, M=2.50 . . . . .	28
17	Interference Axial Pressure Distribution for the M117, M=1.1 . . . . .	30
18	Interference Axial Pressure Distribution for the M117 Store, M=1.3 . . . . .	31
19	Interference Axial Pressure Distribution for the M117 Store, M=1.5 . . . . .	32
20	Surface Velocity Distributions on the Nose Section of the M117 at Mach Numbers of 1.1 and 1.3 . . . . .	35

# LIST OF SYMBOLS

<u>Symbol</u>	<u>Definition*</u>
$a$	Slope of linearly varying line source.
$a_m$	Slope of linearly varying line source at image point.
$A_\infty$	Speed of sound in free stream.
$C_{ld}$	Distance between centerlines of two interfering bodies.
$C_p$	Pressure coefficient.
$h$	Hyperbolic radius.
$m$	Supersonic point source strength.
$M$	Mach number.
$N$	Number of line sources or number of control points.
$r$	Radial coordinate or local body radius.
$S$	Local body slope.
$u$	Perturbation velocity in x direction.
$v$	Perturbation velocity in r direction or in y direction.
$w$	Perturbation velocity in z direction.
$u', v'$	Dimensional perturbation velocities.
$V_s$	Local surface velocity.
$V_\infty$	Free stream velocity.
$x$	Axial coordinate or axial length.
$y$	Coordinate axis.
$z$	Coordinate axis.
$x_o, y_o, z_o$	Coordinates of supersonic point source.

\*All linear dimensions have been nondimensionalized with respect to the M117 max body diameter, 16 inches. All velocities, except where noted, have been nondimensionalized with respect to the free stream velocity,  $V_\infty$ .

LIST OF SYMBOLS (CONCLUDED)

<u>Greek Symbols</u>	<u>Definition</u>
$\alpha$	Angle of attack.
$\delta$	Distance from body centerline to image line.
$\lambda$	Mach number parameter = $\sqrt{M^2 - 1}$ .
$\xi$	Coordinate along line source.
$\sigma$	Transformation variable.
$\phi$	Velocity potential function.



## SECTION I

### INTRODUCTION

Considerable thought was given to the basic approach to be taken in the supersonic analysis of interfering axisymmetric bodies. Initial consideration was given to a source paneling approach since this theory ideally allows one to handle nonaxisymmetric, nonslender bodies of any configuration. Woodward's theory (Reference 1) supposedly is valid for any configuration; however, only source panels which lie parallel to the free stream are applicable to his theory. Additionally, it appears that solutions which could be developed would involve the inversion of large matrices. Consequently, this approach was abandoned in favor of a more flexible solution.

The second approach taken in the analysis was the utilization of linearly varying line source distributions placed along the body centerline to generate the isolated body solution and supersonic point sources strategically placed along the image line as determined by subsonic theory (References 2 and 3) to counteract the presence of adjacent bodies. The basic theory for this analysis is presented in the following sections, but for reasons which will become apparent, this approach fails to adequately model the flow field.

The third approach taken in the analysis is similar to the second approach except, instead of using point sources to counteract the interference effects, linearly varying line source distributions were used. The results and the theory for this technique are also presented in the following sections.



## SECTION II

### ISOLATED BODY SOLUTION

The concept of adding solutions to generate specified body shapes in potential flow is well established in the literature even for linearized supersonic flow (References 4 and 5). In most cases, however, only the essential features of the derivation are presented. For purposes of this investigation, certain elements of the derivation are expanded, or revised, for the interfering body cases. In order to provide good continuity for the whole supersonic analysis, the theoretical derivation for an isolated thin supersonic body is also presented. The approach as presented herein for a thin isolated body closely follows that of Liepmann and Roshko (Reference 4).

#### 1. Theory

The potential for thin bodies in supersonic flow is governed by the well-known wave equation

$$\frac{\partial^2 \phi}{\partial r^2} + \frac{1}{r} \frac{\partial \phi}{\partial r} - \lambda^2 \frac{\partial^2 \phi}{\partial x^2} = 0 \quad (1)$$

It has been shown by von Kármán and Moore (Reference 5) that the potential may be written as an integral over a distribution of sources of the form

$$\phi(x, r) = - \int_0^{x-\lambda r} \frac{f(\xi) d\xi}{\sqrt{(x-\xi)^2 - \lambda^2 r^2}} \quad (2)$$

where field points are represented by  $(x, r)$  and  $\xi$  is the coordinate along the source distribution as shown in Figure 1. Points outside the zone of action or outside the Mach cone produce imaginary solutions for  $\phi$ , and consequently only those points which lie inside the Mach cone are considered.

It is convenient to make a variable transformation of the form

$$\xi = x - \lambda r \cosh \sigma \quad (3)$$

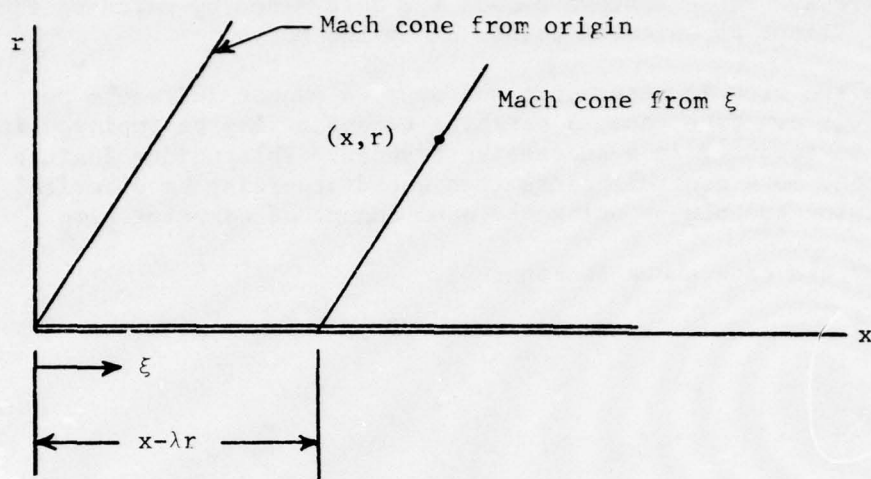


Figure 1. Line Source in Supersonic Flow

in which case the potential reverts to

$$\phi(x, r) = \int_{\sigma = \cosh^{-1}\left(\frac{x}{\lambda r}\right)}^{\sigma=0} f(\xi) d\sigma \quad (4)$$

In Equation (4),  $f(\xi)$  represents the function which governs the strength distribution of the line sources. The simplest source distribution which produces meaningful results is (Reference 4)

$$f(\xi) = a\xi, \quad (5)$$

which obviously is a linearly varying source distribution with zero strength at the nose. For a single source, this solution produces a conical body shape with the flow velocities parallel to the surface everywhere on the body. Since the differential equation is linear, solutions may be added so that an arbitrarily shaped thin axisymmetric body may be generated by

$$f(\xi) = a_1\xi + a_2(\xi - \xi_1) + a_3(\xi - \xi_2) + \dots + a_n(\xi - \xi_{n-1}) \quad (6)$$

The unknowns in Equation (6) are the  $a$ 's which are the respective slopes of the line sources. These unknown slopes are determined by matching flow boundary conditions at selected points along the body.

Because the flow is supersonic and sources cannot influence points upstream of their own Mach cone, a marching technique may be employed in which the  $a$ 's may be computed in a successive fashion. This unique feature allows the use of many more control points than would otherwise be practical for matrix inversion techniques using the same amount of computer time.

Consider the case shown in Figure 2.

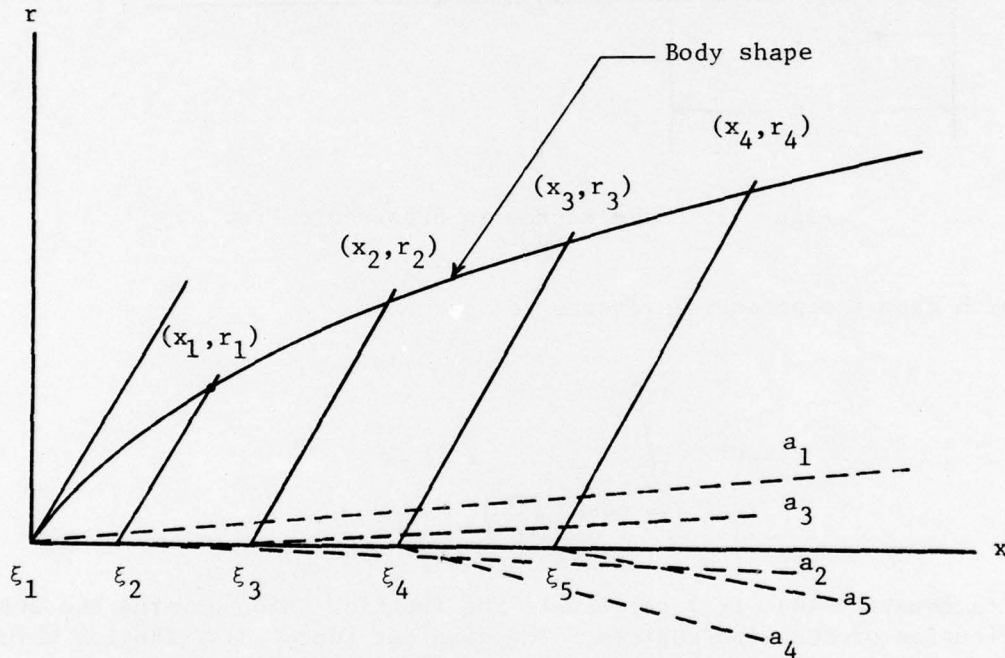


Figure 2. Schematic of the Nose of a Body in Supersonic Flow

As an example, consider the field point  $(x_2, r_2)$ . The line sources which influence  $(x_2, r_2)$  are those associated with  $a_1$  and  $a_2$ . The line source of slope  $a_1$  begins at the nose or at  $\xi_1$ , and the line source of slope  $a_2$  begins at  $\xi_2$ . Note from Figure 2 that the locations of the beginning points of all the line sources are determined from

$$\xi_i = x_i - \lambda r_i, \quad i = 1, 2, 3, \dots, N \quad (7)$$



The potential at any field point affected by  $a_1$  and  $a_2$  is

$$\phi = \phi_{a_1} + \phi_{a_2} \quad (8)$$

and Equation (4) becomes

$$\phi_{a_1} = \int_{\sigma=\cosh^{-1}\left(\frac{x-\xi_1}{\lambda r}\right)}^{\sigma=0} a_1(x-\xi_1 - \lambda r \cosh \sigma) d\sigma \quad (9)$$

The result of the integration is

$$\phi_{a_1} = -a_1(x-\xi_1) \left[ \cosh^{-1}\left(\frac{x-\xi_1}{\lambda r}\right) - \sqrt{1 - \left(\frac{\lambda r}{x-\xi_1}\right)^2} \right]. \quad (10)$$

The potential due to  $a_2$  is

$$\phi_{a_2} = \int_{\xi=\xi_2}^{\xi=\xi} \frac{a_2(\xi-\xi_2)}{\sqrt{(x-\xi)^2 - \lambda^2 r^2}} d\xi \quad (11)$$

Using the variable transformation, Equation (3), the resultant potential is

$$\phi_{a_2} = -a_2(x-\xi_2) \left[ \cosh^{-1}\left(\frac{x-\xi_2}{\lambda r}\right) - \sqrt{1 - \left(\frac{\lambda r}{x-\xi_2}\right)^2} \right], \quad (12)$$

or, in general, the potential due to any  $j$ th line source is

$$\phi_{a_j} = -a_j(x-\xi_j) \left[ \cosh^{-1}\left(\frac{x-\xi_j}{\lambda r}\right) - \sqrt{1 - \left(\frac{\lambda r}{x-\xi_j}\right)^2} \right] \quad (13)$$



The velocity components in the field are found by

$$u = \frac{\partial \phi}{\partial x} = \sum_{j=1}^N \frac{\partial \phi}{\partial x} a_j, \quad (14)$$

and

$$v = \frac{\partial \phi}{\partial r} = \sum_{j=1}^N \frac{\partial \phi}{\partial r} a_j, \quad (15)$$

Results of the differentiation are

$$u = - \sum_{j=1}^N a_j \cosh^{-1} \left( \frac{x - \xi_j}{\lambda r} \right), \quad (16)$$

and

$$v = \lambda \sum_{j=1}^N a_j \sqrt{\left( \frac{x - \xi_j}{\lambda r} \right)^2 - 1}. \quad (17)$$

The points  $(x_1, r_1), (x_2, r_2), \dots, (x_i, r_i)$  as illustrated in Figure 2 are control points where the source strengths  $a_1, a_2, \dots, a_i$  are determined so that the velocity vector is parallel to the local body slope at the control points. As in the subsonic case, the boundary condition is

$$\frac{\Sigma v_i}{1 + \Sigma u_i} = \frac{dr}{dx_i} = S_i \text{ (slope)} \quad (18)$$

For the first control point  $(x_1, r_1)$ , the only influencing line source is due to  $a_1$ . Equation (18) then becomes

$$\frac{\lambda a_1 \sqrt{\left( \frac{x_1 - \xi_1}{\lambda r_1} \right)^2 - 1}}{1 - a_1 \cosh^{-1} \left( \frac{x_1 - \xi_1}{\lambda r_1} \right)} = S_1 \quad (19)$$

Rearranging and solving for  $a_1$  yields

$$a_1 = \frac{S_1}{\lambda \sqrt{\left(\frac{x_1 - \xi_1}{\lambda r_1}\right)^2 - 1} + S_1 \cosh^{-1} \left( \frac{x_1 - \xi_1}{\lambda r_1} \right)} \quad (20)$$

For the second point, the procedure is repeated with the only unknown being  $a_2$  and so on down the body. In general, the solution for the  $i$ th source (slope) strength is

$$a_i = \frac{S_i - \sum_{j=1}^{i-1} \left[ S_i a_j \cosh^{-1} \left( \frac{x_i - \xi_j}{\lambda r_i} \right) + \lambda a_j \sqrt{\left(\frac{x_i - \xi_j}{\lambda r_i}\right)^2 - 1} \right]}{\lambda \sqrt{\left(\frac{x_i - \xi_i}{\lambda r_i}\right)^2 - 1} + S_i \cosh^{-1} \left( \frac{x_i - \xi_i}{\lambda r_i} \right)} \quad (21)$$

From Equation (21), the strength of all the  $N$  line sources are computed at  $N$  control points.

Once all the strengths are known, the isolated body pressure distribution is determined using Equations (16) and (17) as

$$C_p = -2u + \lambda u^2 - v^2 \quad (22)$$

## 2. Results for Body Shape A4V1P

In order to clearly validate the isolated body solution and to provide a check case for the computer program, a thin axisymmetric body was chosen for which pressure data was available in the low supersonic Mach number range. The body so chosen was designated as the A4V1P (Reference 6). Dimensions for the body were nondimensionalized with respect to the M117 maximum body diameter in order to provide a standardized means of comparison. The results for the isolated body for the A4V1P are represented in Figures 3 and 4. Note that the theoretical results are well within experimental error when compared to wind tunnel results. There does seem to be a slight underprediction by the theory in the region of the tail which is probably attributable to buildup of the boundary layer in this region. As a general rule, however, there is excellent agreement between theory and experiment for the isolated A4V1P body.

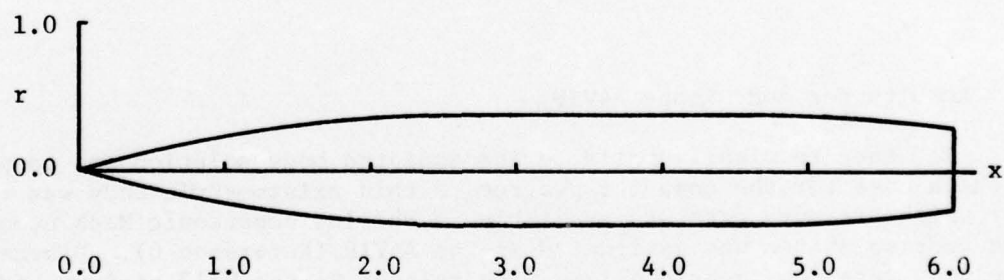
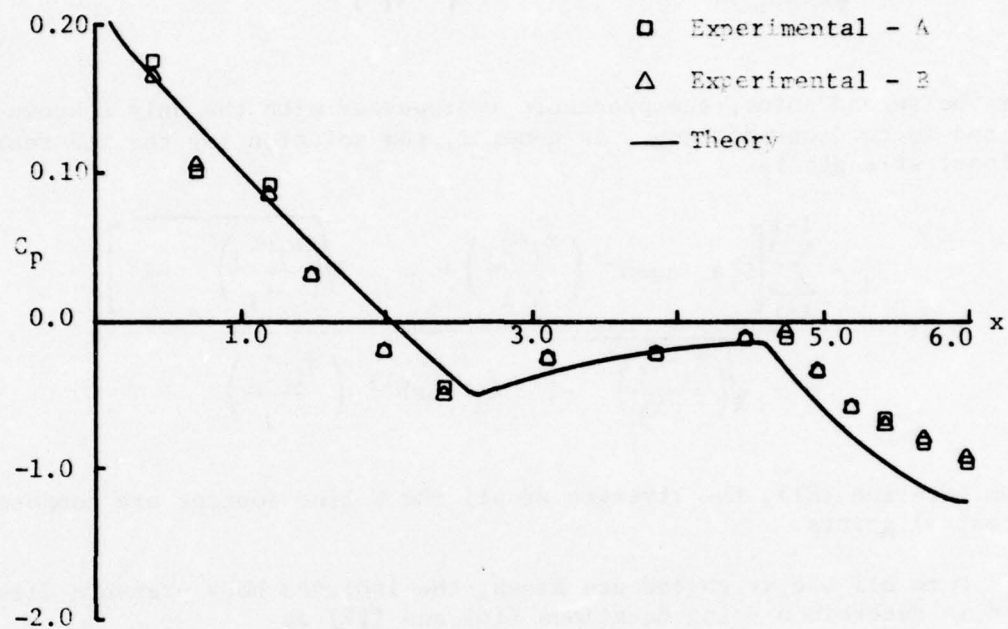


Figure 3. Comparison of Theoretical and Experimental Pressure Distribution for the A4V1P Missile at  $\alpha=0.0$  and  $M=1.87$



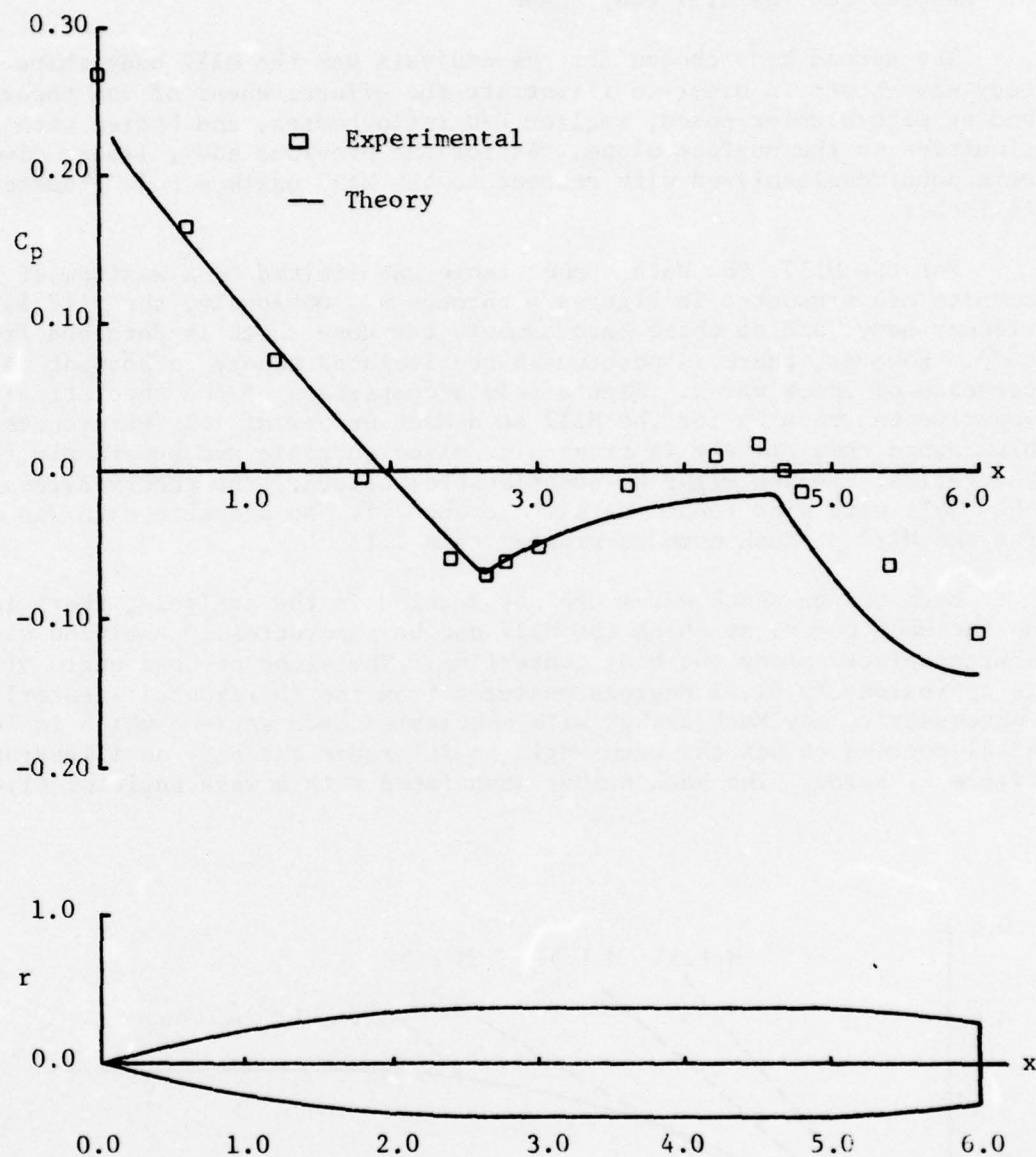


Figure 4. Comparison of Theoretical and Experimental Pressure Distribution for the A4V1P Missile at  $\alpha=0.0$  and  $M=1.56$



### 3. Results for the M117 Body Shape

The second body chosen for the analysis was the M117 body shape. This body was chosen in order to illustrate the effectiveness of the theory for bodies with blunter noses, smaller L/D ratio bodies, and bodies with discontinuities in the surface slope. As for the previous body, linear dimensions were nondimensionalized with respect to the M117 maximum body diameter of 16 inches.

For the M117, the Mach number range was limited to a maximum of 1.5. The results are presented in Figures 6 through 8. Obviously, the M117 is not a slender body, and at these Mach numbers the nose shock is detached from the body. However, there is nothing in the isolated theory to account for the presence of shock waves. Figure 6 is a comparison of the theoretical and experimental results for the M117 at a Mach number of 1.1 (References 7 and 8). Since this clearly is transonic, mixed subsonic and supersonic flows, theoretical results might be questionable; however, the theory agrees remarkably well with wind tunnel data (Reference 7). No pressure data was available for the M117 at Mach numbers greater than 1.1.

Even though shock waves are not modeled in the analysis, there is a limit on the Mach number at which the M117 can be theoretically analyzed with line sources placed along the body centerline. The slope or nose angle of the M117 is approximately 41.41 degrees measured from the (horizontal) centerline axis. Consequently, any Mach number with associated Mach angle  $\beta$  which is less than 41.41 degrees causes the wave angle to intersect the body as illustrated in Figure 5, below. The Mach number associated with a wave angle of 41.41° is

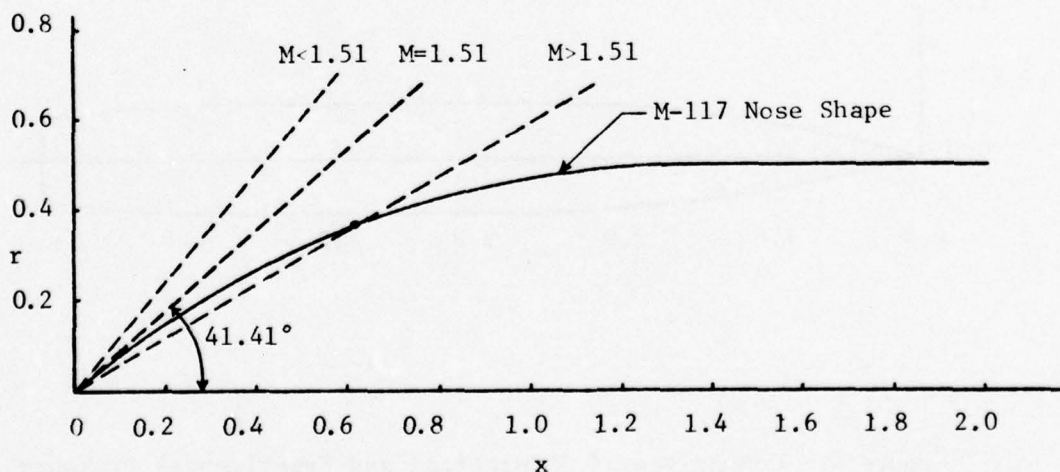


Figure 5. Nose and Centerbody Section of the M117 Store

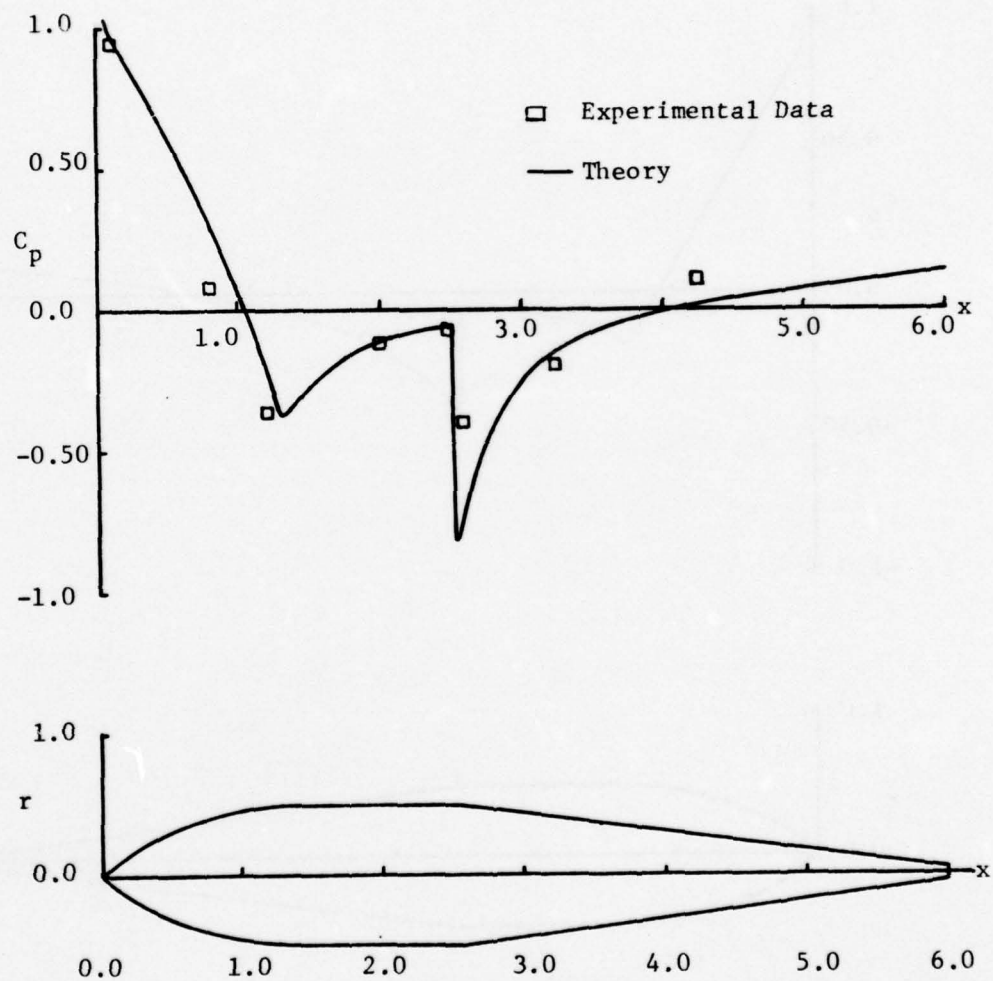


Figure 6. Comparison of Theoretical and Experimental Pressure Distribution for the M117 Store at  $\alpha = 0.0$  and  $M = 1.1$

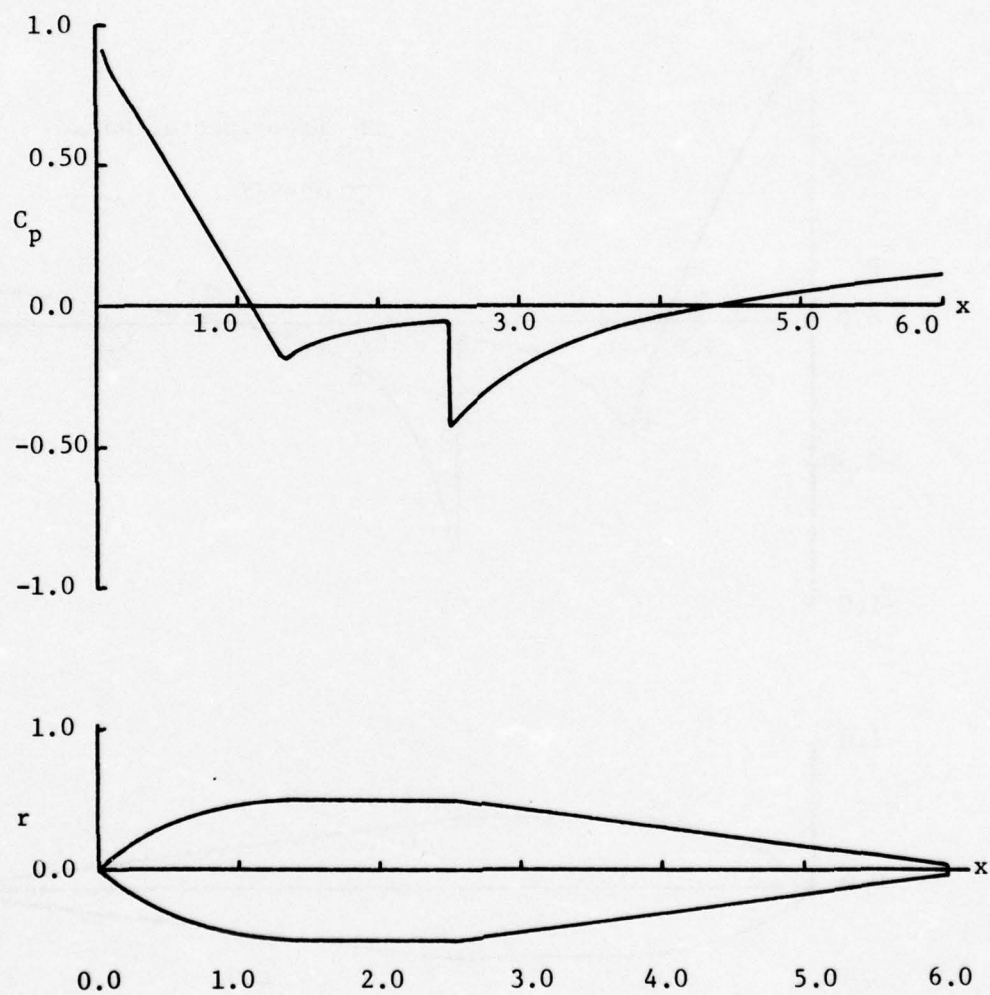


Figure 7. Theoretical Pressure Distribution for the M117 Store  
at  $\alpha = 0.0$  and  $M = 1.3$



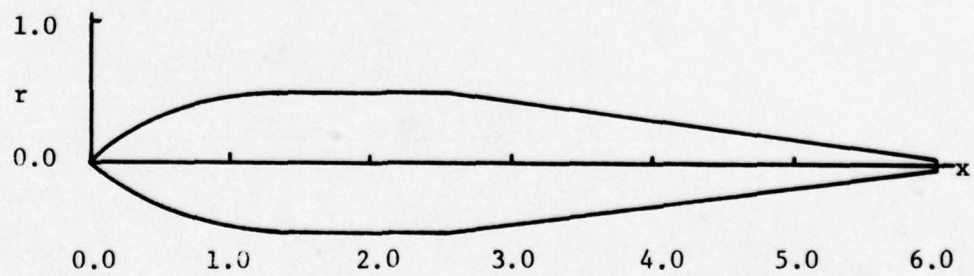
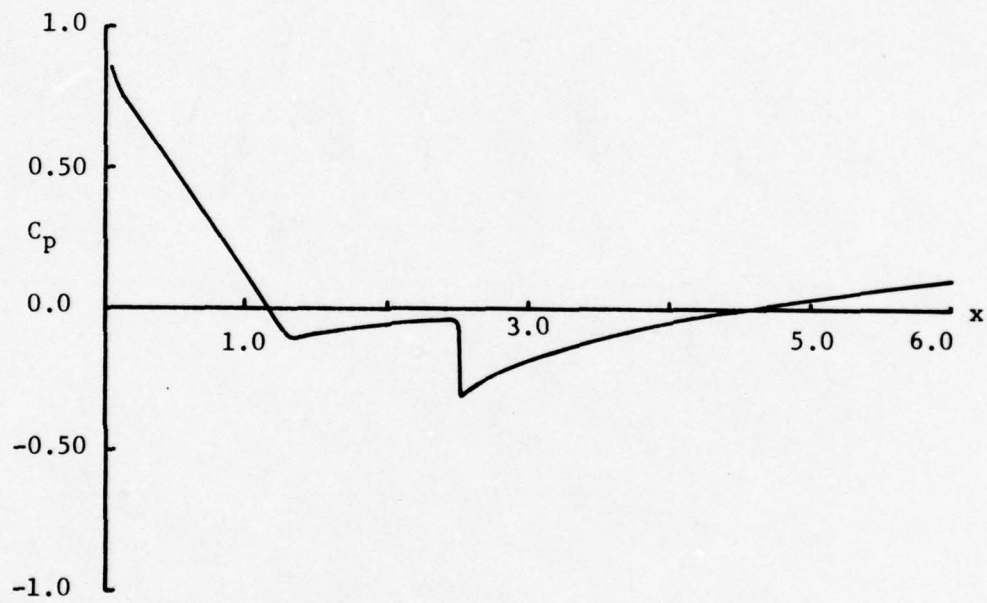


Figure 8. Theoretical Pressure Distribution for the M117 Store at  $\alpha = 0.0$  and  $M = 1.5$

1.51. For Mach numbers greater than 1.51, the associated Mach angle is less than the nose angle; consequently, the theoretical analysis becomes inadequate. For this reason, only Mach numbers up to 1.5 were considered for the M117 store.

In summary, the technique of using line source distributions to model a thin body in supersonic flow is well established. Additionally, the theory as herein applied adequately predicts the basic axial pressure distribution for thin bodies and appears adequate for bodies such as the M117. However, the applicable Mach number range is limited by the nose shape, and for nose shapes blunter than the M117, the Mach number range is severely restricted.

### SECTION III

#### TWO-BODY SOLUTION

There were two attempts to model the two-body interference effects in supersonic flow, the first using a point source image solution and the second using a linearly distributed line source solution. Although the point source solution did not adequately model the flow field, the basic theory and associated results are presented, and the reasons for its failure are also discussed.

##### 1. Point Source Image Solution

For the beginning of the interference problem, it is assumed that the isolated body solution using linearly distributed line sources is completed. For the interference effects, point sources are placed along an image line in each body to counteract the crossflow velocities and maintain the tangency boundary conditions at a set of control points on the surface of each body (see References 2 and 3). The two bodies are arranged as shown in Figure 9. The image line is defined as in subsonic theory as

$$\delta = \frac{C_{ld}}{2} (1.0 - \sqrt{1.0 - (2r/C_{ld})^2}) \quad (23)$$

In order to preserve the short computational time, a scheme was devised so that the marching technique could still be employed for the image system solution as was done for the isolated body solution. Referring to Figure 9, the computational steps proceeded in the following manner.

Geometry - (1) The point labeled "0" on top of body 1 (the lower body) was determined. This is the point on body 1 where the influence of body 2 is first felt. This point is the intersection of the downstream running Mach wave from the nose of body 2 and the top of body 1. (2) Next, the point labeled "1" on the image line of body 1 is determined as the intersection of the upstream running Mach line from the zero point (on top of body 1 just determined) and the image line, as defined in Equation (23), above. This is the point at which the first point source is to be placed. (3) The next step is to determine point 1 on the centerline of body 1 and point zero on the bottom of body 1. The point 1 on the centerline of body 1 is the location of the first sink to approximately counteract the effects of the first source on the image line. (4) Point 1 on the top of body 1 is located at the same axial location as point zero on the bottom of body 1. (5) With point 1 on top of body 1 determined, point 2 on the image line is then determined and the whole process is repeated. As each point in body 1 is determined, the corresponding point in body 2 is also stored in computer memory.



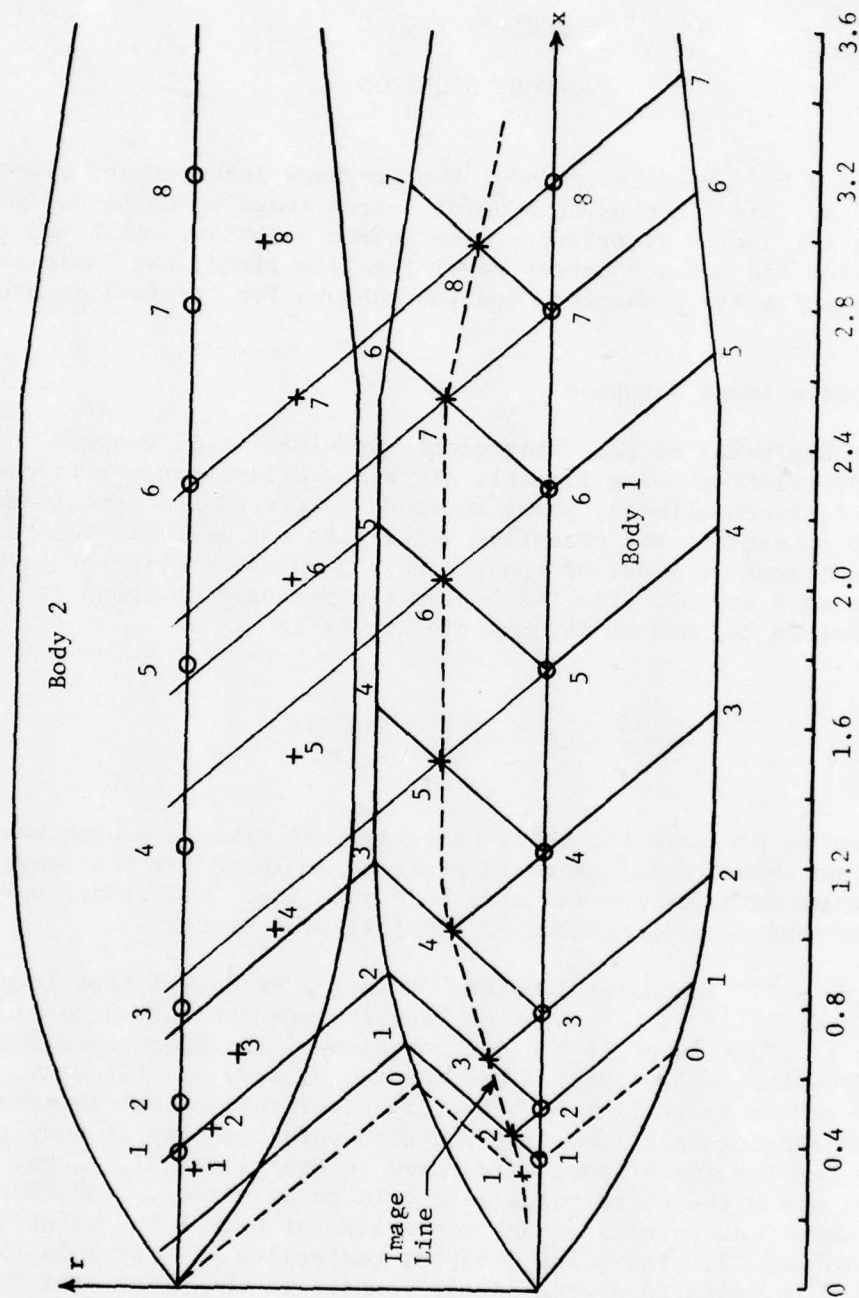


Figure 9. Schematic of Two-Body Interference Geometry Using Point Sources

Computational Procedure - (1) The first control point on top of body 1 is selected. The induced velocities are determined from the line sources in body 2, any point sources in body 2, the line sources in body 1, and any point sources in body 1. From geometry (Figure 9), it is observed that the only unknown point source which can influence the first control point on top of body 1 is the point source located on the image line of body 1; the strength of this point source is determined to maintain flow tangency at the top control point. (2) The first control point on the bottom of body 1 is next selected. The same procedure of determining induced velocities from all upstream line and point sources is followed for this control point on the bottom of body 1. The only unknown point source strength in the upstream running Mach cone from the point 1 (bottom) control point is the one located at the point 1 centerline location. Consequently, the strength of this source is determined to maintain flow tangency on the bottom of body 1 at the first control point. (3) Next, the second control point on top of body 1 is selected, and the strength at the point 2 image location is determined. In this manner alternately selecting control points on top and then on bottom of body 1, the strengths of the point sources located along the image line and along the centerline are respectively determined which forces the flow to be tangent to the body both on top and on bottom of each body at each control point.

Results of Point Source Solution - The resulting solution from the point source analogy hinges on the basic formulation of the induced velocity from a supersonic point source. The potential for a supersonic point source is

$$\phi = - m/h \quad (24)$$

where  $m$  is the source strength and  $h$  is the hyperbolic radius defined by

$$h = \sqrt{(x-x_o)^2 - \lambda^2[(y-y_o)^2 + (z-z_o)^2]} \quad (25)$$

The resulting induced velocities are

$$u = \frac{\partial \phi}{\partial x} = m(x-x_o)/h^3, \quad (26)$$

$$v = \frac{\partial \phi}{\partial y} = - m\lambda^2(y-y_o)/h^3, \quad (27)$$

and

$$w = \frac{\partial \phi}{\partial z} = - m\lambda^2(z-z_o)/h^3. \quad (28)$$

In the above equation,  $x_o, y_o, z_o$  is the location of the source and  $x, y, z$  is the field point.

Two basic observations should be noted from Equations (26) through (28): (a) the induced velocity is dependent on how close the field point is to the source location and (b) the induced velocity is strongly dependent on how close the field point is to the Mach line. As a matter of fact, as the field point gets close to the Mach line,  $h$  approaches zero, and the induced velocity approaches infinity. As clearly illustrated in Figure 9, upstream running Mach lines from the control points come very close to sources in body 2. Consequently, large induced velocities at some of the control points were encountered with a subsequent large source strength to offset the induced velocities. Whenever one exorbitant source strength was determined, each successive strength became larger, thereby causing the solution to blow up. Increasing the number of images and control points only compounds the problem, and reducing the number of images causes exorbitant strengths due to the very wide spacing of the image system. Consequently, this approach was abandoned.

## 2. Line Source Image Solution

As in the point source approach, it is assumed that the isolated body solution has already been completed by placing linearly varying sources along the centerline of each body. The point on body 1 where the nose of body 2 is first felt is determined as before by finding the intersection of the Mach line from the nose of body 2 and the top of body 1. The first control point for the interference system is then selected as the next evenly spaced axial location. For example, in Figure 10, the standard evenly spaced  $x$  locations are 0.2, 0.4, 0.6, 0.8, and so on down the body. The axial location where the interference from the nose of body 2 is first felt on body 1 is approximately 0.54 (Figure 10), designated point "0" on top of body 1. The next evenly spaced axial location is 0.6, which is designated as point 1 on the top of body 1 and point 0 on the bottom. Evenly spaced axial locations, 0.8, 1.0, 1.2, ..., are then selected to define other downstream control point locations on each body.

Note from Figure 10 that the location of the first image line source is the intersection of the upstream running Mach line from point 0 on top of body 1 and the upstream running Mach line from point 0 on the bottom of body 1. In order to more clearly illustrate the geometry associated with the computational system, Figure 11 is a schematic of the nose section of one of the interfering bodies as illustrated on Figure 10. The axial distance to the beginning point of the image line is designated as  $\xi_m$  and from Figure 11,

$$\xi_{m_k} = [x_{k-1} - \lambda(r_{k-1} - \delta_k)]_{\text{top}} \quad (29a)$$

$$= [x_{k-1} - \lambda(r_{k-1} + \delta_k)]_{\text{bot}} \quad (29b)$$



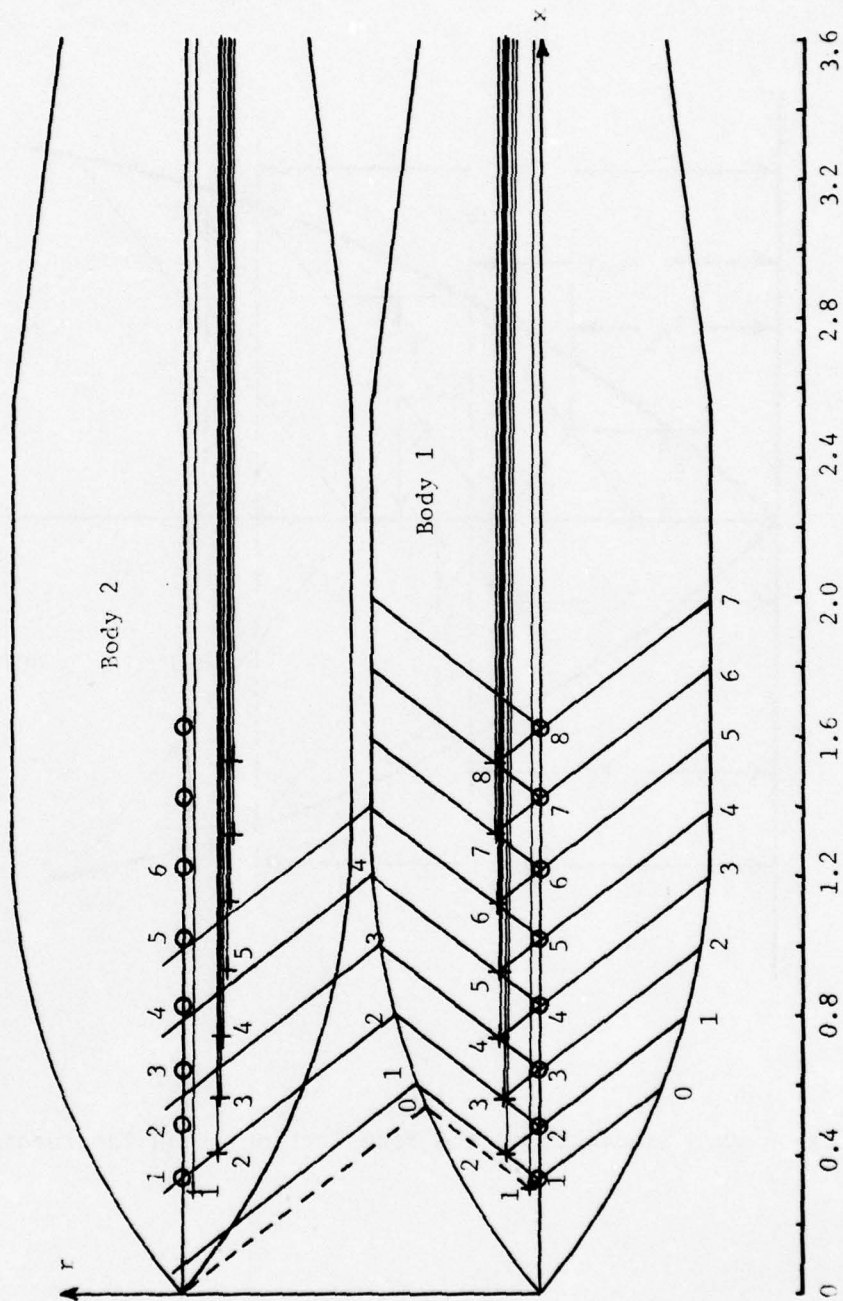


Figure 10. Schematic of Two-Body Interference Geometry Using Line Sources

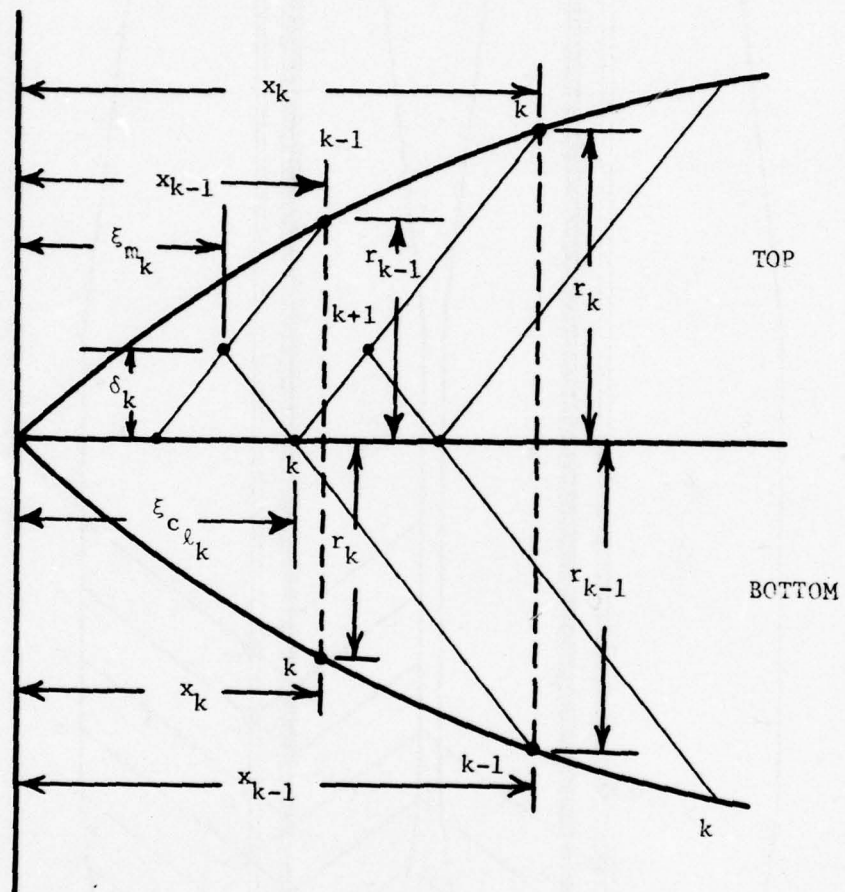


Figure 11. Schematic of the Nose Section of an Intersecting Body

where  $\delta_k$  is the radial distance from the body centerline to the  $k$ th image point. Note from Figure 11 that

$$(x_{k-1})_{\text{bot}} = (x_k)_{\text{top}} \quad (30a)$$

and

$$(r_{k-1})_{\text{bot}} = (r_k)_{\text{top}}. \quad (30b)$$

From Equations (29) and (30), then

$$\delta_k = \frac{1}{2} [(x_k - x_{k-1})/\lambda + (r_{k-1} - r_k)] . \quad (31)$$

Each line source extends from its point of origin, as defined by Equations (29) and (31), to infinity and is parallel to the  $x$  axis as shown in Figure 10. As the origin of each line source location is determined for body 1, corresponding locations in body 2 are also stored in computer memory. Note that the location of the image line is determined by the  $\Delta x$  interval chosen for the computations and not from a predetermined equation. Actually, this poses no problem because velocities induced from linearly varying line sources are constant along any Mach line emanating from the line source, i.e.,  $(x/\lambda r) = \text{constant}$ .

The locations of the beginning point of the centerline line sinks are determined from Figure 11 as

$$(\xi_{c_\ell})_k = x_k - \lambda r_k . \quad (32)$$

These sinks along the centerline are used to match boundary conditions on the bottom of body 1 due to the presence of body 2.

The equations which govern the induced velocities from these line sources are basically Equations (16) and (17) which are slightly modified as

$$u_i = - \sum_{j=1}^N a_{m_j} \cosh^{-1} \left( \frac{x_i - \xi_{m_j}}{\lambda r_{p_{ij}}} \right) \quad (33)$$

and

$$v_i = \lambda \sum_{j=1}^N a_{m_j} \sqrt{\left( \frac{x_i - \xi_{m_j}}{\lambda r_{p_{ij}}} \right)^2 - 1} \quad (34)$$



where  $r_{p_{ij}}$  is the radial distance between the control point and the beginning of  $p_{ij}$  the line source ( $i$  = control point). It should be noted from the geometry, as illustrated on Figure 10, that a marching technique can be utilized to find the unknown strengths of the image sources to match boundary conditions on top of body 1 and the unknown sink strengths placed along the body centerline to match boundary conditions on the bottom of body 1.

One additional restraint is placed on the marching scheme from Figure 10; consider, as an example, control point designated number 3 on top of body 1. Note that the upstream running Mach line from this control point encounters the image line source number 3 in both body 1 and body 2. Since this double encounter may or may not occur for any one particular control point, provisions must be made in the computational procedure to include the double induced velocity for the affected control points. The technique used in this analysis is outlined below. (1) An array is set up in the computer which contains the strength of the image line sources. This array is initially set up with zeros stored in all of its locations. (2) As each line strength is determined, the corresponding zero is replaced by the computed line source strength. (3) Control points as previously determined are successively chosen in a downstream marching fashion. Consider as an example the  $k$ th control point. The induced velocity from all line sources in the upstream running Mach cone is determined with the only unknown (appearing in both bodies) being the  $k$ th line source strength  $a_{m_k}$ . The boundary condition then becomes

$$\frac{v_k + V_r}{1 + u_k + V_x} = S_k \text{ (slope)} \quad (35)$$

where  $V_r$  and  $V_x$  are the accumulated sum of the radial and axial velocity components of all known line sources in the upstream Mach cone of the  $k$ th control point.

From Equations (33) and (34) and taking into account the double encounter effect, the axial and radial induced velocities from the  $k$ th line source become, respectively,

$$u_k = -a_{m_k} \left[ \cosh^{-1} \left( \frac{x_k - \xi_{m_k}}{\lambda r_{p_{kk}}} \right) \right]_{\text{body 1}} - a_{m_k} \left[ \cosh^{-1} \left( \frac{x_k - \xi_{m_k}}{\lambda r_{p_{kk}}} \right) \right]_{\text{body 2}} \quad (36)$$

and

$$v_k = \lambda a_{m_k} \left[ \sqrt{\left( \frac{x_k - \xi_{m_k}}{\lambda r_{p_{kk}}} \right)^2 - 1} \right]_{\text{body 1}} - \lambda a_{m_k} \left[ \sqrt{\left( \frac{x_k - \xi_{m_k}}{\lambda r_{p_{kk}}} \right)^2 - 1} \right]_{\text{body 2}} \quad (37)$$

From Equations (35), (36) and (37), the line strength is isolated as

$$a_{m_k} = \frac{S_k(1.0 + v_x) - v_r}{\lambda k_1 + S_k k_2} \quad (38)$$

In the above equation,

$$k_1 = \sqrt{G_1^2 - 1} - \sqrt{G_2^2 - 1} \quad (39)$$

$$k_2 = \cosh^{-1} G_1 + \cosh^{-1} G_2 \quad (40)$$

where

$$G_1 = [(x-\xi)/(\lambda r)]_{\text{Body 1}} \quad (41)$$

and

$$G_2 = [(x-\xi)/(\lambda r)]_{\text{Body 2}} \quad (42)$$

For control points where the double encounter is not a problem, it may be shown that

$$a_{m_k} = \frac{S_k(1.0 + v_x) - v_r}{\lambda \sqrt{G_1^2 - 1} + \cosh^{-1} G_1} \quad (43)$$

Centerline strengths are determined in a similar manner to match boundary conditions on the bottom of body 1. The results of the computations for the interference solution are presented in the next section.

### 3. Results for Body Shape A4V1P

For the A4V1P, it was necessary to assume some spatial centerline distance for the two interfering bodies. Since there was no experimental data for comparison purposes, the nondimensional centerline distance was chosen to be 1.0. This choice provided good interference effects even on the nose of the two bodies.

The results for the interference pressure distribution is shown on Figures 12 through 16. The angular locations refer to body 1 (bottom body) with boundary conditions being matched exactly on top of body 1 (90°) and on bottom of body 1 (-90°).

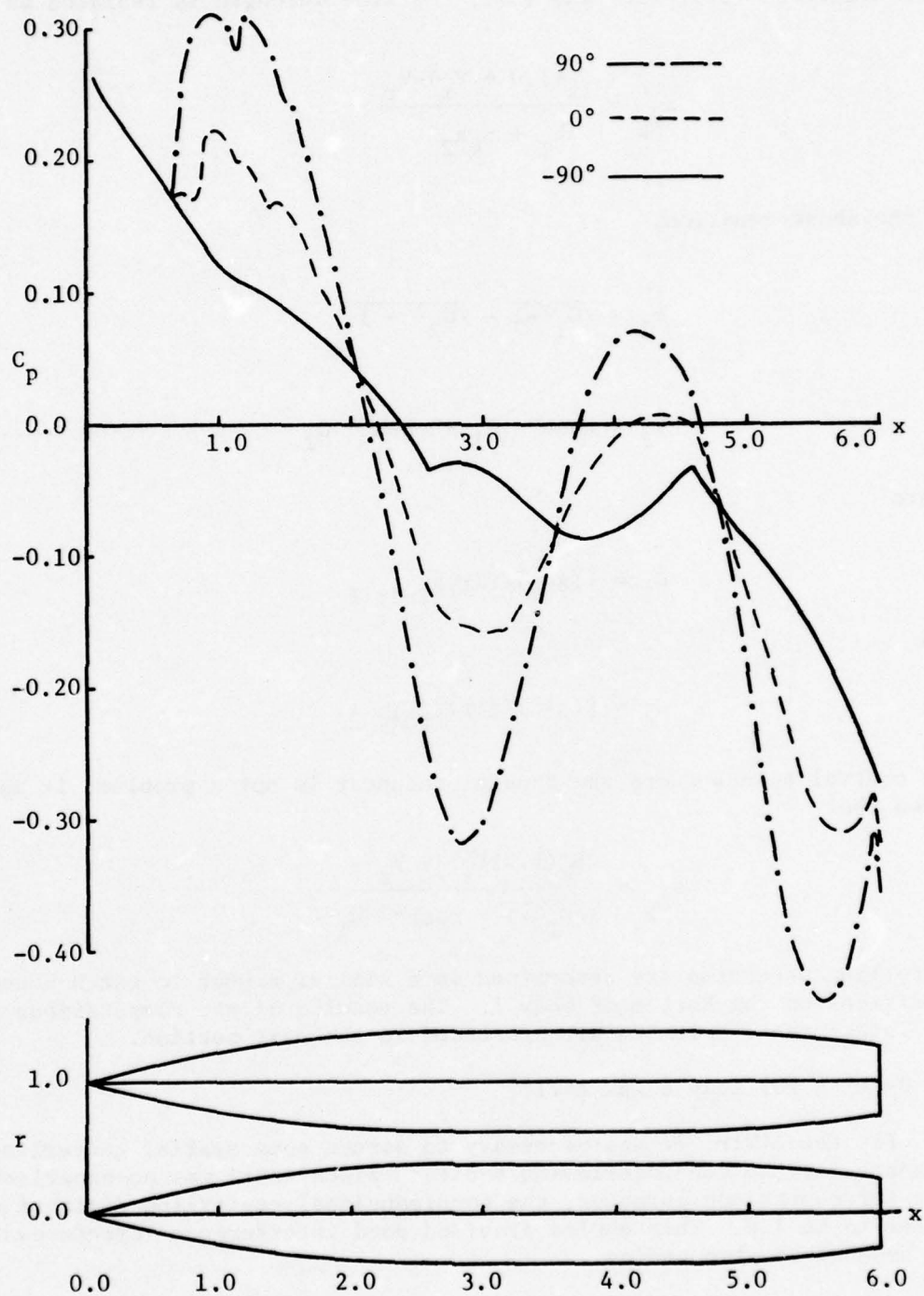


Figure 12. Interference Axial Pressure Distribution for the A4V1P,  $M = 1.30$



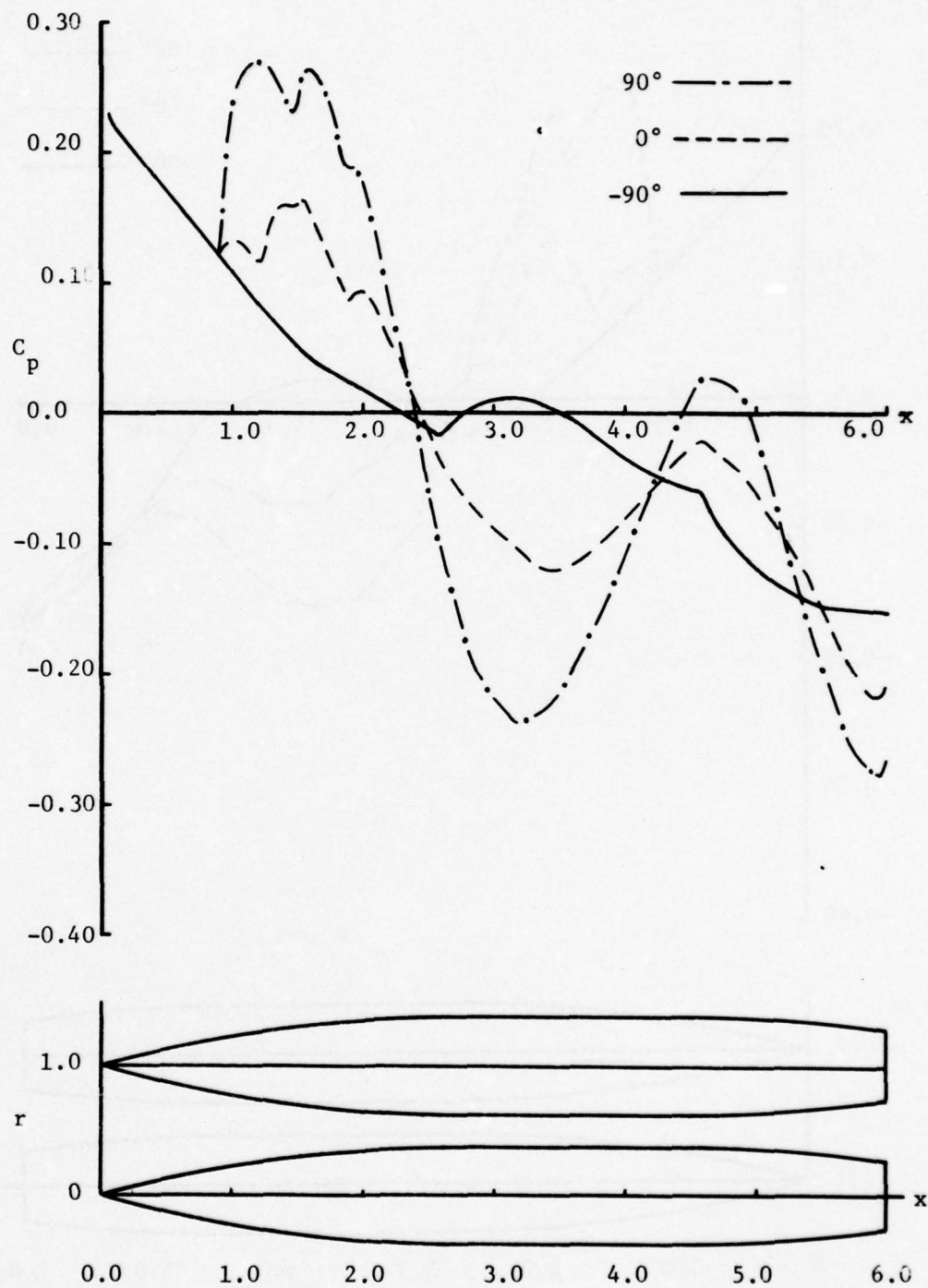


Figure 13. Interference Axial Pressure Distribution for the A4V1P,  $M = 1.56$

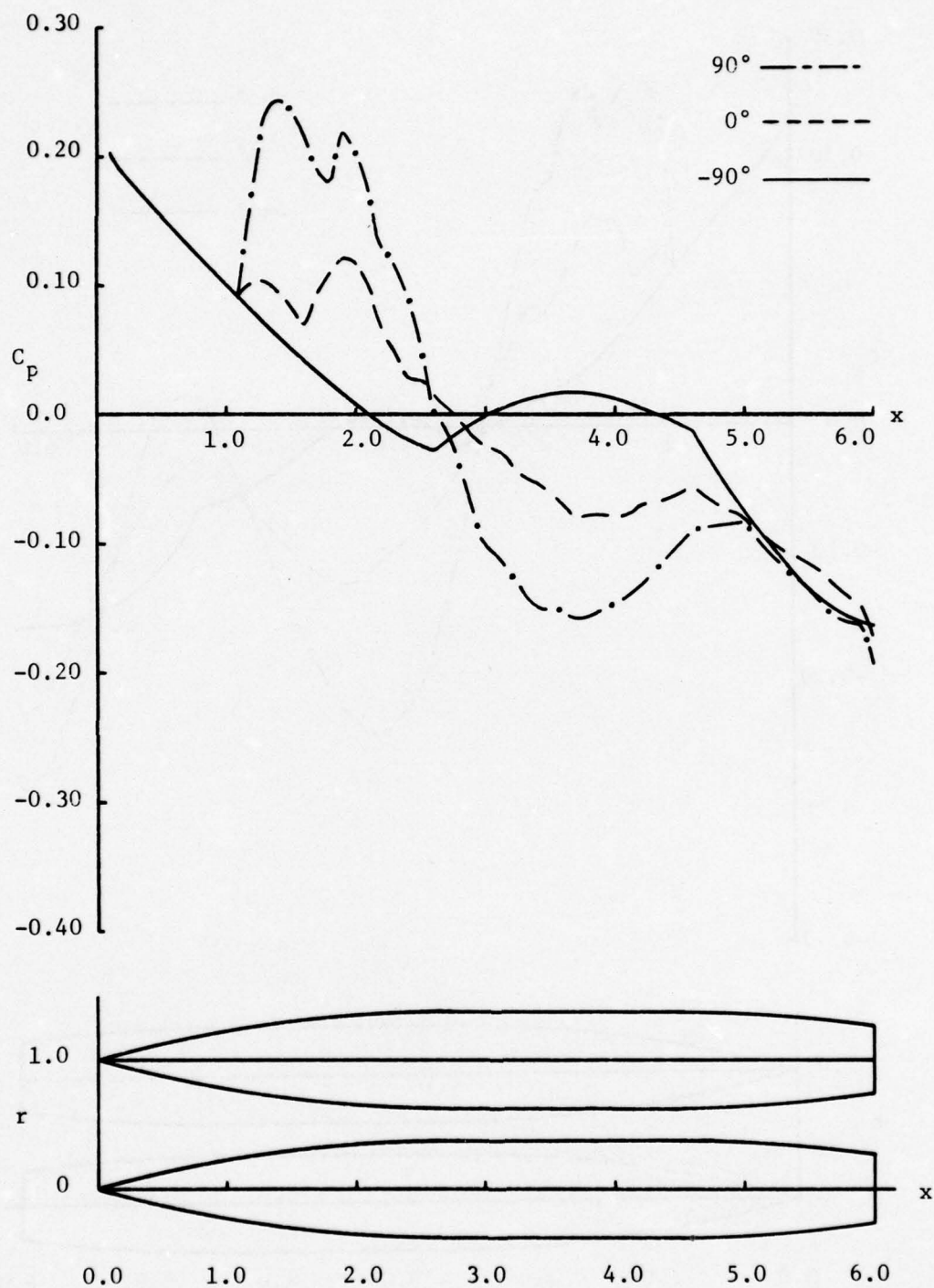


Figure 14. Interference Axial Pressure Distribution for the A4V1P,  $M = 1.87$ , 60 Line Sources

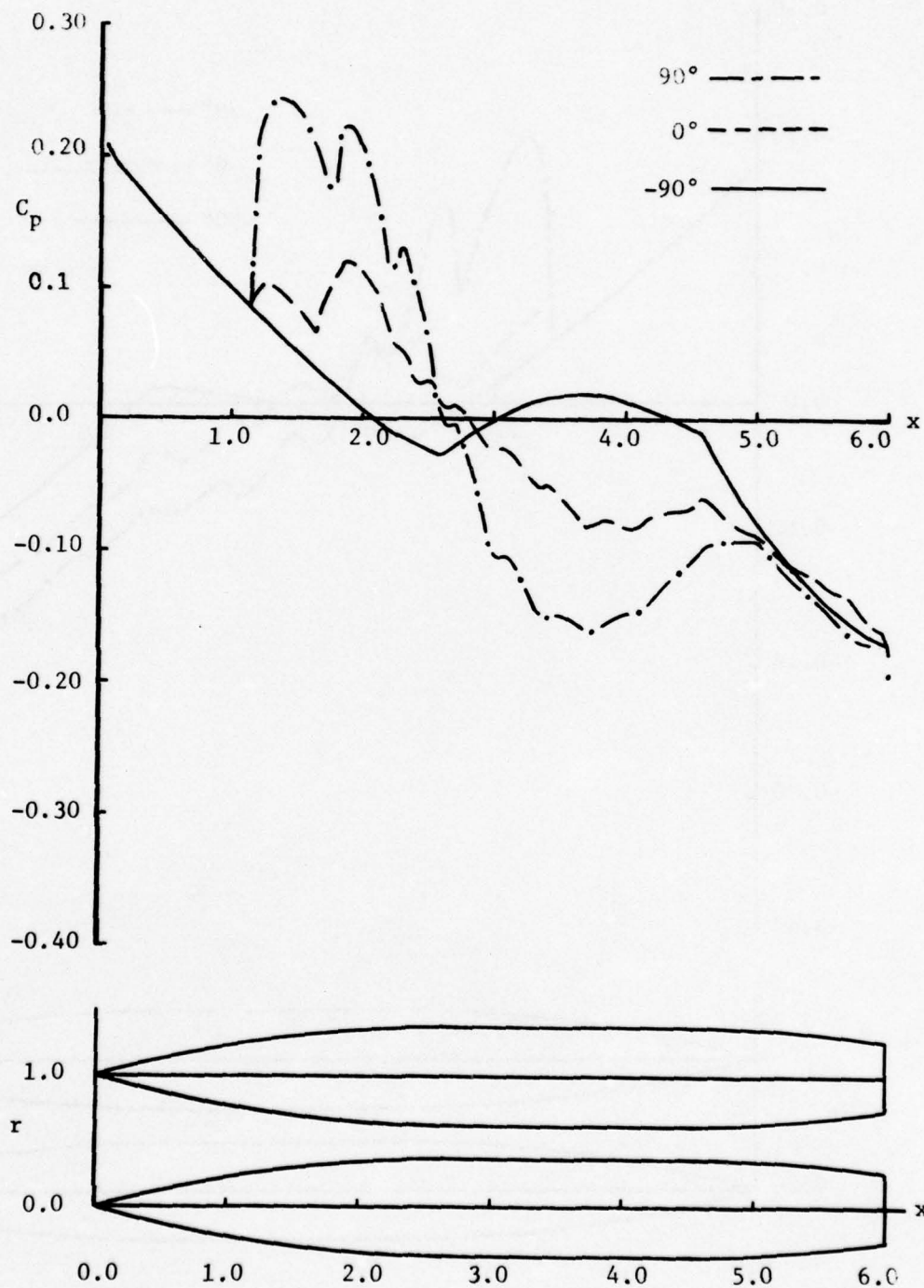


Figure 15. Interference Axial Pressure Distribution for the A4V1P,  $M = 1.87$ , 120 Line Sources



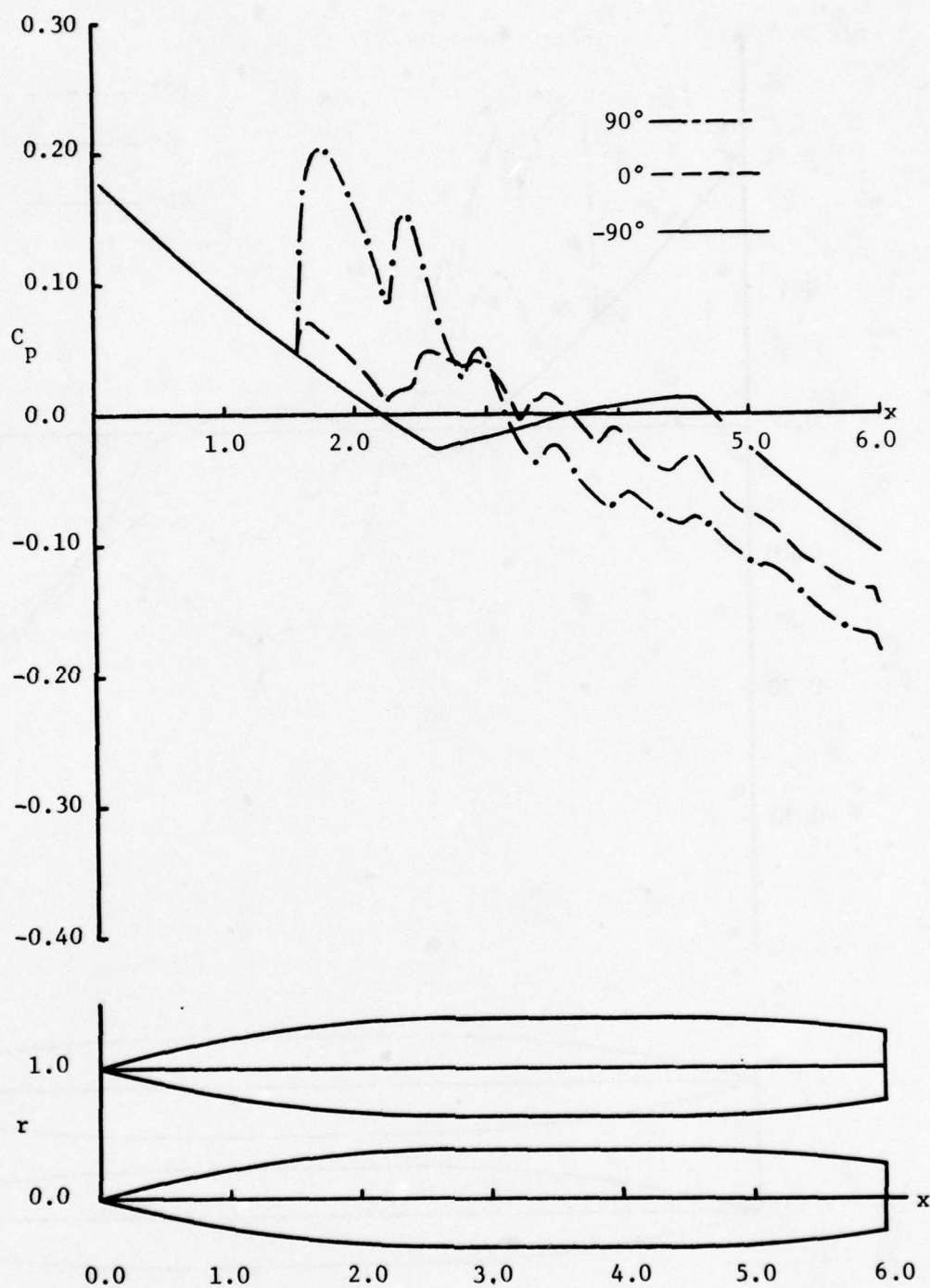


Figure 16. Interference Axial Pressure Distribution for the A4V1P,  $M = 2.50$

To lend credence to the formulation of the problem and the resulting solution, the  $-90^\circ$  case, bottom of body 1 on Figure 14 or 15, is very nearly the same as the free stream data as illustrated in Figure 3. As the two bodies interfere with each other, the pressure on top of body 1 begins to increase, meaning that the flow is slowing down or approaching  $M=1.0$ . One would expect this result since the flow is converging between the bodies. Note also that the resulting pressure distribution on the body produces a very large negative pitching moment which is in agreement with experimental results for stores of similar shape. However, since no actual interference data for the A4V1P is available, comparison of the magnitude of the numbers for the interference case is not possible.

It has previously been stated that the radial position of the image line has no influence on the induced velocities. Also, from the derivation of the interference equations, the radial position of the image line is determined by the  $\Delta x$  interval chosen for the analysis. In order to clearly illustrate this point, Figure 14 is the interference results using 60 line sources and Figure 15 is the interference results using 120 line sources. The difference in the pressure distributions from these two runs are of minor magnitudes as expected.

Since the A4V1P is indeed a slender body, the theoretical results were well behaved with pressure distributions much as expected. Because the M117 is not a slender body and because of the maximum Mach number limit encountered on the nose for the isolated body solution as previously discussed, one might expect additional problems for interfering M117 stores.

#### 4. Results for the M117 Body Shape

The problem of the limited Mach number range for the M117 associated with the nose geometry of course still existed for the interference cases. In addition to the nose angle problem, the computations for the flow over the sharp shoulder proved to be somewhat of a problem for the interfering case. In the real situation, an expansion fan must exist at the shoulder if the flow is to remain supersonic. However, the free stream flow must possess a sufficiently high Mach number if it is to make the turn without separating or shocking down. For the isolated body (M117), this problem did not emerge from the solution as is shown in Figures 5 through 7; however, for the two-body case, the mathematical analysis does indeed become unstable when computations are attempted downstream of the shoulder.

In Figures 17 through 19, the results for the interference calculations for two adjacent M117 stores are presented. The centerline distance is 1.042 diameters as is approximately the case when the stores are mounted on the triple ejector rack (TER). Note that for these plots the scale on the pressure distribution is an order of magnitude smaller than on the A4V1P results. Note also that the computations for  $C_p$  were limited to  $\pm 2.0$  since pressure coefficients outside this range are completely unrealistic.

At very low supersonic Mach numbers (Figure 17), the computational technique becomes unstable aft of the sharp shoulder. From physical

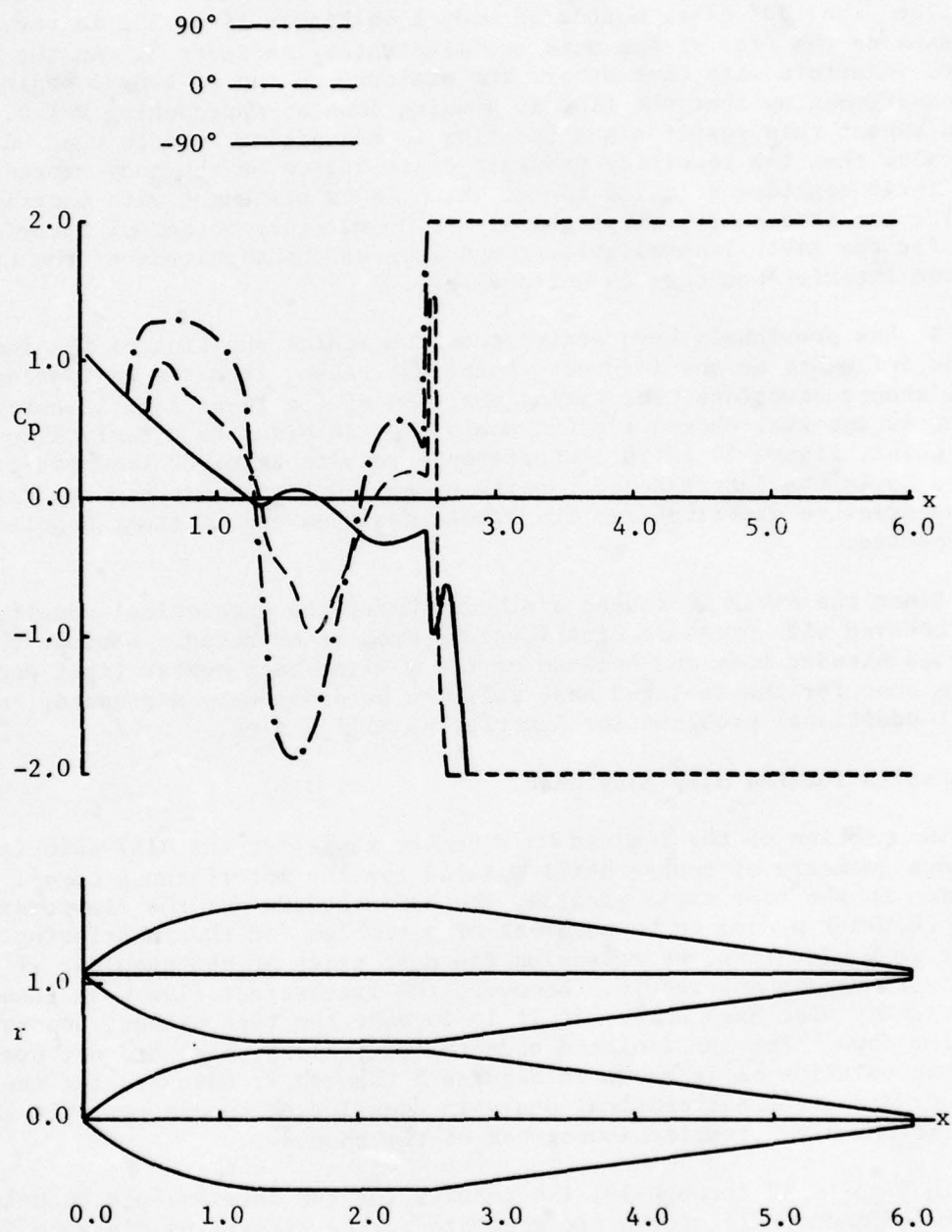


Figure 17. Interference Axial Pressure Distribution for the M117 Store,  $M = 1.1$



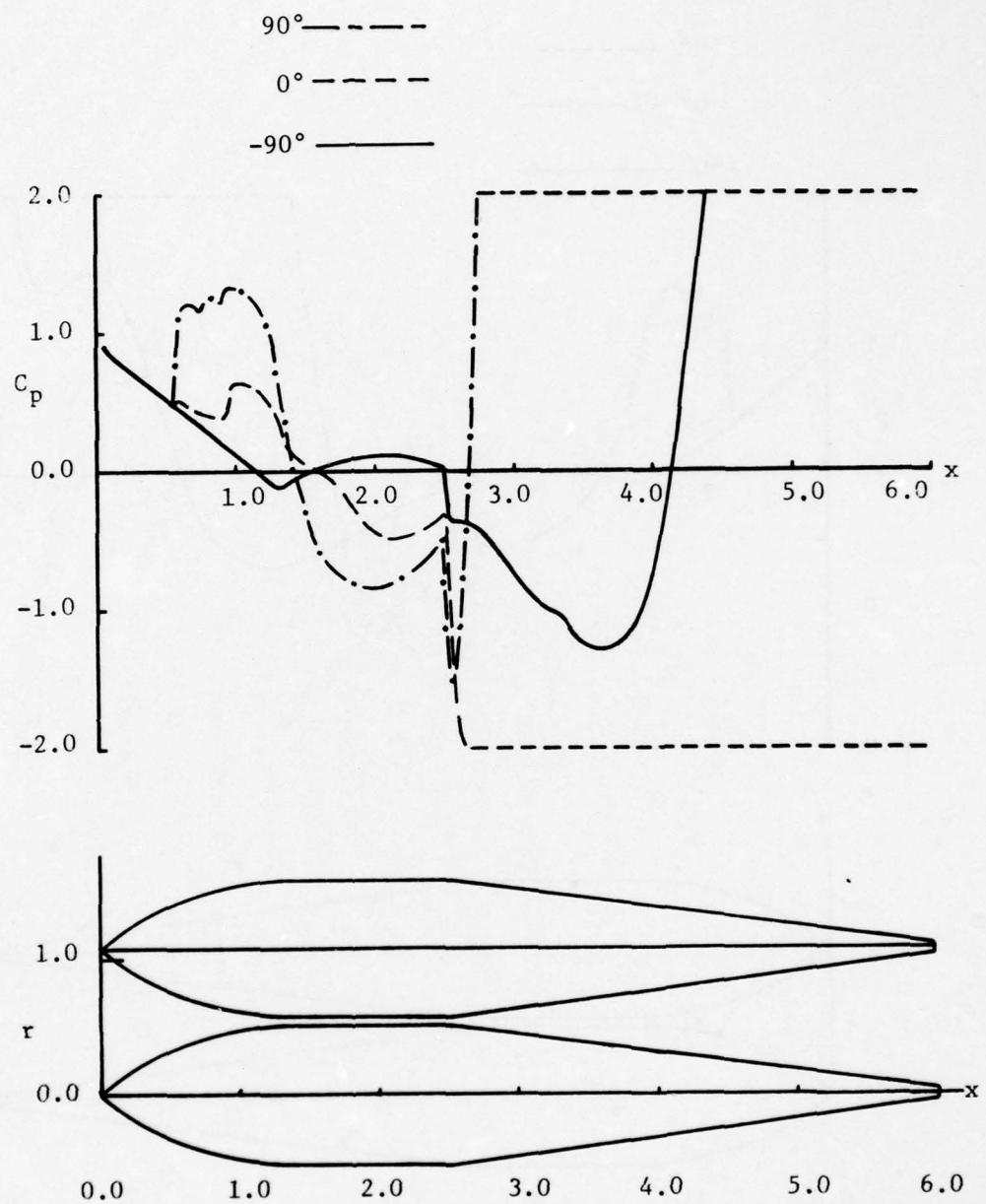


Figure 18. Interference Axial Pressure Distribution for the M117 Store,  $M = 1.3$

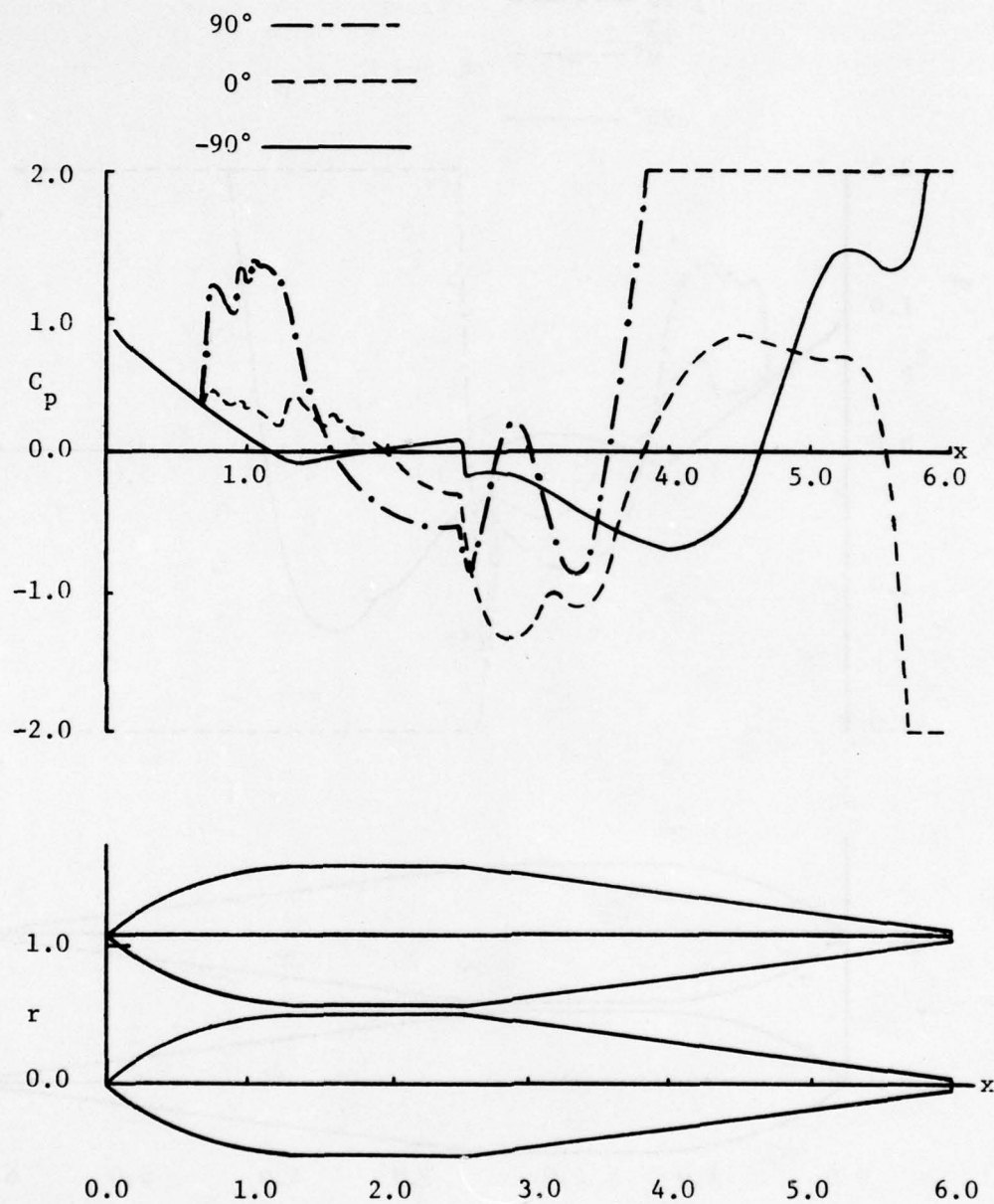


Figure 19. Interference Axial Pressure Distribution for the M117 Store,  $M = 1.5$

principles of the flow between adjacent bodies, some pressure recovery mechanism such as a standing normal shock is necessary for low supersonic Mach numbers. Since this mechanism is not incorporated in this analysis, the solution becomes unstable. This instability is also seen in Figures 18 and 19. Note, however, as the free stream Mach number increases ( $M=1.5$ ), the point on the body where the solution becomes unstable moves downstream of the shoulder.

Specific conclusions regarding the agreement of the theory with experimental data were not possible since no data for a two-store M117 configuration was available.

#### 5. Surface Velocities on the M117

Another interesting aspect of these theoretical results for the M117 emerged from the computations. In the analysis it is assumed that small perturbation theory is applicable. Therefore, the velocity induced from the line sources must be much less than the free stream velocity. From Equation (16) it is noted that, for a linearly varying line source, the axial component of the velocity is negative. Consequently, at small Mach numbers, i.e.,  $M=1.1$ , even small perturbations may generate subsonic surface velocities. If the perturbation velocities are to maintain supersonic flow on the body surface, then

$$(V_{\infty} + u')^2 + (v')^2 > A_{\infty}^2 \quad (44)$$

Nondimensionalizing with respect to  $V_{\infty}$  yields

$$(1 + u)^2 + v^2 > 1/M_{\infty}^2 \quad (45)$$

The left-hand side of Equation (45) is the nondimensional surface velocity, or

$$V_s = \sqrt{(1 + u)^2 + v^2} \quad (46)$$

For supersonic flow on the body surface, then

$$V_s > \frac{1}{M_{\infty}} \quad (47)$$

As an example, for  $M=1.1$ , Equation (47) becomes

$$V_s > .9091 \quad (48)$$



Figure 20 is a plot of the nondimensionalized surface velocity,  $V_s$ , for the M117 at Mach numbers of 1.1 and 1.3. This figure and Equation (47) indicate that subsonic flow must exist over certain portions of the nose if the body boundary conditions are to be met. This simple analysis also theoretically predicts the sonic point on the nose and the subsequent region of supersonic flow.

The predicted areas of subsonic and supersonic flow appear realistic; however, it should be stressed here that the authors do not imply that the results are rigorous and certainly many other factors should be included in the analysis. If, however, the results were taken literally, then the nose section of the M117 should be treated with a subsonic analysis and the aft section with supersonic analysis. Future work in this area could result in one program that could perhaps handle both situations or, in essence, provide a simplified transonic solution.

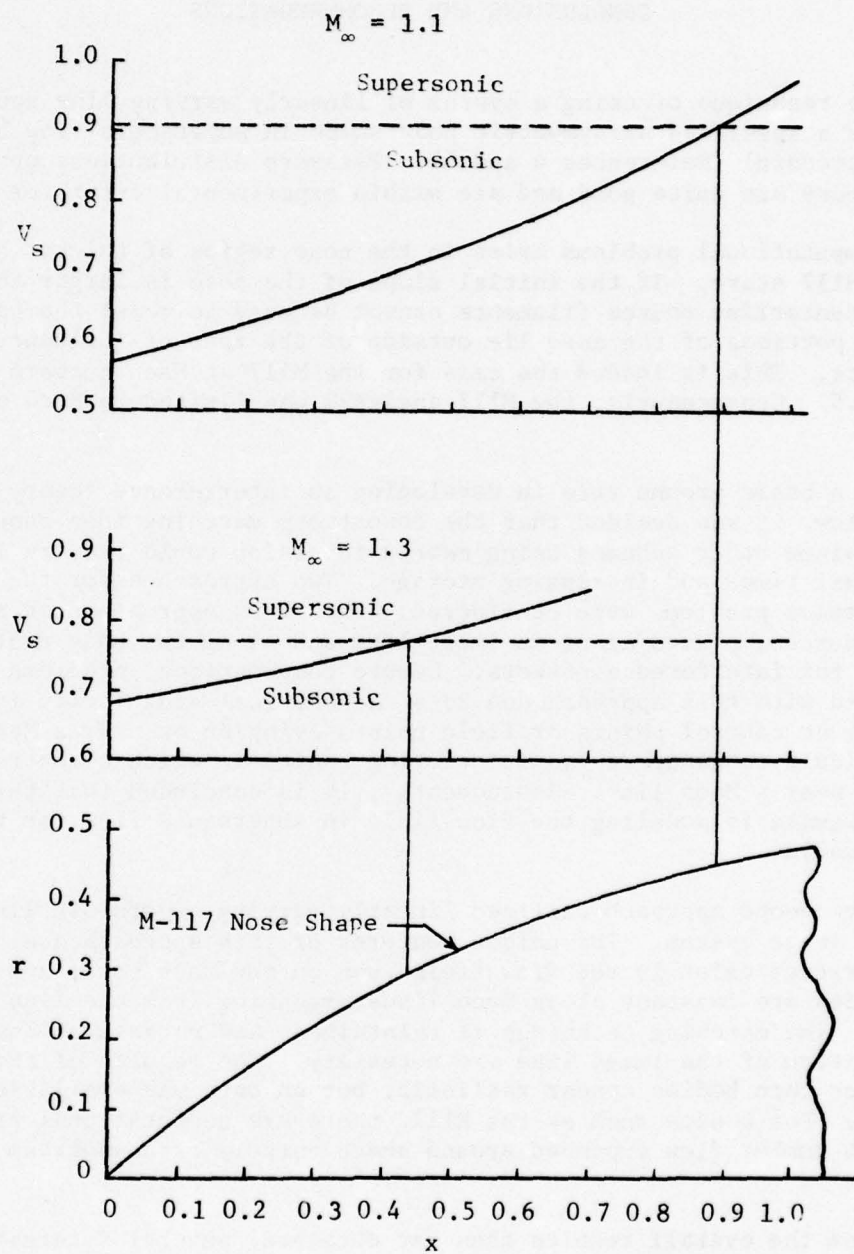


Figure 20. Surface Velocity Distributions on the Nose Section of the M117 at Mach Numbers of 1.1 and 1.3

## SECTION IV

### CONCLUSIONS AND RECOMMENDATIONS

The technique of using a system of linearly varying line sources to generate a specified axisymmetric body shape in supersonic flow has proven very successful (References 4 and 5). Pressure distributions obtained from this theory are quite good and are within experimental error for thin bodies.

Computational problems arise in the nose region of thicker bodies such as the M117 store. If the initial slope of the nose is larger than the Mach angle, centerline source filaments cannot be used to model the body shape because portions of the nose lie outside of the zone of influence of the filaments. This is indeed the case for the M117 at Mach numbers greater than about 1.5. Consequently, the M117 analysis was limited to Mach numbers below 1.5.

As a basic ground rule in developing an interference theory for supersonic flow, it was decided that the downstream marching idea should be maintained since other schemes using matrix inversion would require longer computational times and increasing storage. Two approaches for the supersonic interference problems were considered. The first approach used supersonic point sources, placed along an image line and along the body centerline, to account for interference effects. Severe computational problems were encountered with this approach due to a mathematical singularity in the induced velocity at control points or field points lying on or near a Mach line. It is difficult to generate two interfering bodies in which a control point does not lie near a Mach line. Consequently, it is concluded that this approach is inadequate in modeling the flow field in supersonic flow for two interfering bodies.

The second approach utilized linearly varying supersonic line sources for the image system. The unique features of this approach are: (1) no singularities exist in the flow field even on the Mach cone, and (2) induced velocities are constant along Mach lines emanating from the line source itself. The marching technique is maintained, and no assumptions concerning the location of the image line are necessary. The results of these computations for thin bodies appear realistic, but no data was available for comparison. For bodies such as the M117, there are computational problems when low Mach number flow expanded around sharp corners or downstream of sharp corners.

From the overall results thus far obtained, several interesting concepts or recommendations have emerged:

1. The idea of using supersonic line sources and perhaps line doublets to model interfering bodies appears promising.



2. Experimental pressure data for two interfering bodies should be obtained to verify the analysis.

3. Extension of the theory to include some boundary layer effects is necessary.

4. Theoretical approaches for determining the Mach number distribution over the nose section of blunt interfering bodies must be developed.

5. The potential theory technique for identifying subsonic and supersonic flow regions should be pursued and more rigorously founded in theory.

6. A complete program for handling simultaneously both subsonic and supersonic flow regimes on a single body needs to be developed as an initial effort in the solutions of the transonic flow field.

#### REFERENCES

1. Woodward, Frank A., "Analysis and Design of Wing-Body Combinations at Subsonic and Supersonic Speeds," AIAA Journal of Aircraft, November-December 1968, Vol. 5, No. 6.
2. Martin, Fred W., Saunders, Grady H., Smith, Charles J., "Image System Solution for Store Aerodynamics with Interference - Part I," AIAA Journal of Aircraft, March 1975, Vol. 12, No. 3, pp. 151-155.
3. Martin, Fred W., Walkley, Kenneth B., "Image System Solution for Store Aerodynamics with Interference - Part II," AIAA Journal of Aircraft, March 1975, Vol. 12, No. 3, pp. 156-161.
4. Liepmann, H. W., and A. Roshko, Elements of Gasdynamics, John Wiley & Sons, Inc., New York, 1962, pp. 226-239.
5. Von Kármán, T., and N. B. Moore, "The Resistance of Slender Bodies Moving with Supersonic Velocities with Special Reference to Projectiles," Trans. A.S.M.E., Vol. 54, 1932, pp. 303-310.
6. Thompson, J. R., "A Rapid Graphical Method for Computing the Pressure Distribution at Supersonic Speeds on a Slender Arbitrary Body of Revolution," NACA TN 1768, Jan. 1949, pp. 23-24.
7. Mattasits, G. R., "Aerodynamic Interference Effects on Various Weapons Shapes in the Flow Field of a Transonic Wing Configuration at Numbers from .5 to 1.3," Report No. AECD-TR-75-92, or AFATL-TR-75-88, July 1975.
8. Martin, Fred W., Burkhalter, John E., and Cutchins, Malcolm A., "Summary and Analysis of Wind Tunnel Tests of Several Store Configurations at High Subsonic and Low Supersonic Speeds," AFATL-TR-76-22, March 1976.

APPENDIX A  
COMPUTER PROGRAM DOCUMENTATION



# LIST OF VARIABLES

Variable	
<u>Name</u>	<u>Definition</u>
A	Slope of linearly varying line sources for the isolated body.
ACL1	Slope of linearly varying line sources for the centerline image strengths in body 1.
ACL2	Slope of linearly varying line sources for the centerline image strengths in body 2.
AM1	Slope of linearly varying line sources for the image strengths in body 1.
AM2	Slope of linearly varying line sources for the image strengths in body 2.
CLD	Nondimensional distance between body centerlines for two interfering bodies.
CP	Pressure coefficient.
IPLOT	INPUT variable. If IPLOT is input as 0, no plots are obtained. If it is input as 1, plots are obtained.
L1	Axial coordinate nondimensional distance from the nose of the body to the first shoulder (end of ogive nose section).
L2	Axial nondimensional distance from nose of body to second shoulder (end of cylindrical section).
L3	Axial nondimensional coordinate length of body.
M	Mach number.
N	Number of centerline sources to be placed in the body.
NCP	Number of axial points on the body at which the pressure is to be computed.
NPLOT	Number of azimuthal locations around the body at which pressure computations are to be made. The angular increments are every 45°.
R	Local radius of body.

# LIST OF VARIABLES (CONCLUDED)

<u>Variable Name</u>	<u>Definition</u>
RCL1	Radial distance from the coordinate x-axis to the centerline images in body 1 (RCL1 = 0.0).
RCL2	Radial distance from coordinate x-axis to centerline image sources of body 2 (RCL2 = CLD)
RIS1	Radial distance from x-axis to image line of body 1.
RIS2	Radial distance from the coordinate x-axis to the image line in body 2.
RMAX	Maximum body radius in nondimensional units.
S	Local slope of body.
SI	Axial distance from coordinate axis to beginning point of centerline line sources.
TANG	Tail angle of M117 in degrees.
TAN2	Tangent of tail angle on the M117.
THAD	Azimuthal angle around body at which the first set of pressures are to be computed.
VR	Local radial nondimensional velocity component.
VX	Local axial nondimensional velocity component.
X	Axial distance along the body.
XCL	Axial distance to beginning point of centerline images in body 1 or body 2.
XIS	Axial distance from coordinate axis to beginning point of image line sources.

## INTRODUCTION

A copy of the computer program used in the interference analysis is included in this appendix. The case as illustrated in the program listing is for the M117 store at Mach 1.3. A brief discussion of each subroutine is included below with required inputs. A listing of the major variables in the program is also included.

### MAIN

The executive part of the program calls the required subroutines which perform various tasks to determine, ultimately, the pressure distribution on two interfering bodies. The general sequence of events which MAIN performs is as follows: (1) Sets up the geometry for a single body solution. (2) Generates the single body line source solution. (3) Sets up locations of the image sources, along image line and body centerline for the two-body interfering case. (4) Determines the coordinates of the point where body 2 first interferes with body 1. (5) Generates the interfering body solution for the image source strengths and the image centerline source strengths. (6) Determines the pressure distribution on the body at selected coordinate locations. (7) Plots desired results.

The inputs to MAIN are in the form of data cards as shown on the next page. This information is passed to the various subroutines through labeled COMMON blocks as listed at the beginning of MAIN.

### SUBROUTINE GEOMB (RAD, X, SLOPE, NS)

The GEOMB subroutine determines the local body radius and body slope at discrete axial locations. The axial locations enter the subroutine through the CALL argument list as the X array. The array which contains corresponding body radii is the RAD array, and the SLOPE array contains the corresponding body slopes. These arrays are transferred back through the CALL argument list. Other necessary input parameters for GEOMB enter through the COMMON statement. The variable NS in the CALL argument list is the number of axial locations contained in the X array. Other variables have already been identified in the main program.

### SUBROUTINE RHP (K, X, R, XI, RI, THA, ACC)

The RHP subroutine determines how many of the line sources in body 1 or 2 influence any particular control point under consideration. This number is transferred back through the CALL argument list as K. Other arrays which are transferred to RHP through the CALL are X, R, XI, and RI. These arrays are generated elsewhere in the program. The variable THA in the CALL argument is the azimuthal angle around the body at which the control point is located, and ACC is the desired accuracy of how close a line source is to



Enter in a field of F10.0 the value of THAD.  
 Enter in the next 2 fields of I2 (Starting  
 in column 11) the value of IPLOT and NPLOT.

-90.0 0005

Enter 2 fields of I3 the values of N  
 and NCP. On the same card enter in  
 the next 2 fields of F10.0 the Mach  
 number and the 2-body centerline  
 distance spacing

060060 1.3 1.042

Enter in 7 fields of F10.0,  
 the values of L1, L2, L3,  
 RMAX, TANG, A4VLP, M117.

1.32278 2.54375 6.0 .50 7.50 0.0 1.0

Note: If the M117 is to be  
 run, the field for A4VLP  
 should have 0.0 in it and  
 the field for M117 should  
 have 1.0. If the A4VLP is  
 to be run, then, A4VLP=1.0  
 and M117=0.0.

an upstream running Mach line before it is excluded from consideration. Usually, this number is set equal to approximately .00001. Internal to Subroutine RHP, the variable RHP is the square of the hyperbolic radius of the upstream running Mach cone emanating from the control point under consideration.

SUBROUTINE VELOT (K, X, R, XO, RO, AM, VX, VR, THA)

Subroutine VELOT determines the induced velocity at a control point (X,R) located on body 1 due to all applicable image line sources in body 2, centerline image sources in body 2, image sources in body 1 and centerline image sources in body 1. The velocity components are summed and transferred back as VX and VR in the CALL argument list. The arrays XO, RO, and AM are generated elsewhere in the program and are transferred into and out of VELOT through the CALL argument list. The variables X and R designate the axial and radial coordinate location of the control point under consideration, and THA has the same meaning as in Subroutine RHP. The arrays XO and RO contain the axial and radial location of the line sources in the upstreams running Mach cone from (X,R), and AM contains the strengths of these line sources.

SUBROUTINE VELI (K, X, R, SI, A, VX, VR, THA)

This subroutine determines the induced velocity at the control point (X,R) on body 1 due to the distributed line sources (single body solution) in body 1. All variables have been previously defined with input information entering through the CALL argument list.

SUBROUTINE VELIT (K, X, R, SI, A, VX, VR, THA)

This subroutine is essentially the same as VELI except it determines the induced velocities at the control point (X,R) on body 1 due to the distributed line sources (single body solution) in body 2.

SUBROUTINE VELOCY (VX, VR, TT, XX, THA)

This subroutine is the sub-executive program for determining induced velocities at the various control points. It calls the other required subroutines and transfers the summed velocity components and VX and VR back to the MAIN program. The control point location under consideration is (XX,TT).

```

REAL M,L3,LMD,L1,L2,M117,KN
DIMENSIONX(C62),R(C60),S(C60),XT(C60),RT(C6C),ST(C60)
DIMENSION CPA(20),CPB(2C),XE(2C),CP(C62)
COMMON/CC/SI(C60),A(C60),RCL2(C60),XIS(C60),RIS1(C60),
*AM2(C60),XCL(C60),ACL2(C6C),AM1(C6C),RCL1(C60),ACL1(C60),
*RIS2(C60)
COMMON/AA/N,LMD,CLD
COMMON/B/L1,L2,L3,RMAX,TAN2,A4VIP,M117,YTL
21 FORMAT(8X,1FX,12X,1HR,13X,1HS)
22 FORMAT (1X,3F14.6)
29 FORMAT (1X,13,4X,4HVR =F 9.4,4X,4HVX =F 9.4,4X,4HRC =F 9.4,
*4X,3HS =F9.4,4X,7HERRCR =F9.4,4X,4HCP =F12.4,4X,3FX =F9.4)
30 FORMAT(1X,2FA(13,3H) =F14.6)
40 FORMAT(1X,15HNC OF SOURCES =13,5X,23HNC OF PRESSURE PCINTS =
*13,5X,9FMACH NC =F1C.3,5X,5HCLC =F1C.4)
501 FORMAT (1X,4F2C.5,10X,12)
READ(5,111) L1,L2,L3,RMAX,TANG,A4VIP,M117
111 FORMAT(7F1C.0)
WRITE(6,112) L1,L2,L3,RMAX,TANG,A4VIP,M117
112 FCRMAT(7F1C.6)
READ(5,2) N,NCP,M,CLD
2 FORMAT (13,13,F1C.0,F10.C)
9 READ(5,7) TAC,IPLOT,NPLOT
7 FCRMAT(F1C.C,2I2)
WRITE(6,4C) N,NCP,M,CLD
YO=(L1**2-RMAX**2)/(2.0*RMAX)
YTL=((7.17860-L2)**2-RMAX**2)/(2.0*RMAX)
TAN2=TANG/57.29578
LMD=SQRT(M*M-1.0)
XLMS=LMD*LMD
QN=FLOAT(N)
CX=L3/QN
X(1)=0X
DO 20 J=2,N
X(J)=X(J-1)+0X
20 CONTINUE
CALL GEOME(R,X,S,N)
WRITE(6,21)
C WRITE(6,22)(X(J),R(J),S(J),J=1,N)
N1=N-1
SI(1)=0.0
DO 3 J=2,N
SI(J)=X(J-1)-LMD*R(J-1)
C WRITE(6,49) J,SI(J)
C 49 FORMAT (5X,12,10X,F14.6)
3 CONTINUE
DO 4 I=1,N
SUM=0.0

```



```

      IF(I.EQ.1) GO TO 330
      J1=I-1
      DO 5 J=1,J1
      U=(X(I)-SI(J))/(LMC*R(I))
      C=ALCC(U+SCRT(L*U-1.0))
      SUM=SUM+S(I)*A(J)*C+LMD*A(J)*SCRT(L*U-1.0)
5    CCNTINUE
      XNUM=S(I)-SUM
      U1=(X(I)-SI(I))/(LMC*R(I))
      GC TC 350
330  U1=X(1)/(LMC*R(1))
      XNUM=R(1)/X(1)
      S(1)=XNUM
350  DENCN=LMD*SCRT(U1*U1-1.0) +S(1)*ALOG(L1+SCRT(L1*U1-1.0))
      A(1)=XNUM/DENCN
      WRITE(6,30) I,A(I)
4    CCNTINUE
C    STORE LOCATIONS AND STRENGTHS OF IMAGE SOURCES IN BODY 1
C    AND BODY 2 AT END OF BODIES.
      DO 50 J=1,N
      XIS(J)=6.0
      RIS1(J)=.04
      RIS2(J)=CLC-.04
      AM1(J)=C.C
      AM2(J)=0.0
C    THE 1 AND 2 IN THE VARIABLES IDENTIFIED ABOVE REFER TO
C    BODY 1 AND 2 RESPECTIVELY.
50  CCNTINUE
C    STORE LOCATIONS AND STRENGTHS OF CENTERLINE SOURCES IN
C    BODY 1 AND 2 AT THE END OF THE BODIES.
      DO 51 J=1,N
      XCL(J)=6.0
      RCL1(J)=0.0
      RCL2(J)=CLC
      ACL1(J)=C.C
      ACL2(J)=0.0
51  CCNTINUE
      IF(CLC.GT.4.0) GC TC 14
      I=1
C    WE MUST NOW DETERMINE WHERE ON BODY 1 THE NOSE OF BODY 2
C    FIRST INTERFERES WITH BODY 1.
      RP=CLC
      XP=C.0
C    IF A POINT ON BODY 2 IS GIVEN (XP,RP) THIS SECTION OF THE
C    PROGRAM CALCULATES THE INTERSECTION OF THE DOWNSTREAM
C    RUNNING MACH LINE FROM (XP,RP) AND THE UPPER SURFACE OF
C    BODY 1. THIS INTERSECTION POINT IS CALCULATED AS (XIS,RIS)
C

```

```

C      IF KN IS SET = 1.0 , THE POINT ON TCP OF THE BODY IS
C      COMPUTED. IF KN IS SET = -1.0 , THE POINT ON THE BOTTOM
C      OF THE BODY IS COMPUTED.
      KN=1.0
      XIN=XP+(L1/RMAX)*((LMC*CLC)/(LMC+(L1/RMAX)))
      WRITE(6,113) XIN
113  FORMAT(4F,XIN=,F10.6)
      70 KCNT=1
      Y=XIN
      80 IF(XIN.LT.L1) RIN=-YC+SQRT((L1**2+YC**2)-(L1-X(I))**2)
      IF(XIN.GT.L1.AND.XIN.LT.L2) RIN=RMAX
      IF(XIN.GT.L2) GO TO 14
      XNEW=XP+LMC*(RP-KN*RIN)
      IF(ABS(XIN-XNEW).LT.CCCCC1) GO TO 210
      DIF2=XIN-XNEW
      IF(KCNT.EQ.2) GO TO 190
      DIF1=DIF2
      XIN=XNEW
      KCNT = KCNT+1
      GO TO 80
190  XIN=(DIF1*XIN-DIF2*Y)/(DIF1-DIF2)
      GO TO 70
210  IF(KN.LT.0) RIN=-RIN
      XIN=XNEW
      NAP=1
      WRITE(6,501) XP,RP,XIN,RIN,NAP
      DO 60 J=1,N
      IF(XIN.GT.X(J)) GO TO 60
      JSAVE = J
      XTSAVE=X(J)
      RTSAVE=R(J)
      SSAVE=S(J)
      WRITE(6,69) JSAVE,XTSAVE,RTSAVE,SSAVE
69  FORMAT(5X,I3,5X,3F14.6)
      GO TO 62
60  CONTINUE
62  XT(I)=XTSAVE
      RT(I)=RTSAVE
      ST(I)=SSAVE
      RIS1(I)=.5*((XTSAVE-XS)/LMD+(RS-RTSAVE))
      XIS(I)=XS-LMC*(RS-RIS1(I))
      XCL(I)=XT(I)-LMD*RT(I)
      RIS2(I)=CLC-RIS1(I)
      IP=JSAVE+1
      WRITE(6,505)
505  FORMAT(15X,3F,XIS,17X,3HRIS,17X,3HXCL,12X,IHI)
      WRITE(6,504)XIS(I),RIS1(I),XCL(I),I

```

```

504 FORMAT(1X,3F20.6,110)
55 I2=I+1
   XT(I2)=X(IP)
   RT(I2)=R(IP)
   ST(I2)=S(IP)
   RIS1(I2)=.5*((XT(I2)-XT(I))/LMD+(RT(I)-RT(I2)))
   XIS(I2)=XT(I)-LMD*(RT(I)-RIS1(I2))
   XCL(I2)=XT(I2)-LMD*RT(I2)
   RIS2(I2)=CLC-RIS1(I2)
   WRITE(6,504)XIS(I2),RIS1(I2),XCL(I2),I2
   IF(XT(I2).GT.5.99) GO TO 56
   I=I+1
   IP=IP+1
   GC TC 55
56 JAP=I
   WRITE(6,66)
66 FORMAT(12X,2HXM,12X,2HRM,12X,3HXFH,11X,2HXX,12X,2HTT,12X,
*3HAM1,11X,2HXB,12X,2HBB,11X,4HACL1)
   CC 100 J= 1, JAP
   VX = C.0
   VR = 0.0
   XX=XT(J)
   TT=RT(J)
   XB=XT(J+1)
   BB= RT(J+1)
   IF(TT.LT.RIS1(J)) GC TO 100
   CALL VELCCY (VX,VR,TT,XX,1.570796)
   IF(ABS(VX).LT..CCCCC1) GC TO 101
C   NOTE AT THIS POINT J IS THE NUMBER OF THE CONTROL POINT
C   THAT IS FIRST AFFECTED BY THE PRESENCE OF THE OTHER BODY.
   XM=XX-XIS(J)
   RM=RIS2(J)-TT
   XFH=XM*XM-LMD*LMD*RM*RM
   XNUM=ST(J)*(1.C+VX)-VR
   AG=XM/(LMD*(TT-RIS1(J)))
   SRT=SQRT(AG*AG-1.0)
   IF(XFH)63,63,64
63 AM1(J)=XNUM/(LMD*SRT+ST(J)*ALCG(AG+SRT))
   GC TC 65
64 AGG=XM/(LMD*(RIS2(J)-TT))
   SRTT=SQRT(AGG*AGG-1.0)
   RCC=LMD*(SRT-SRTT)
   RCC=ALCG((AGG+SRTT)*(AG+SRT))
   AM1(J)=XNUM/(RCC+ST(J)*RCC)
65 AM2(J)=AM1(J)
C   WE NOW CONSIDER THE CONTROL POINT ON THE BOTTOM OF BODY 1.
101 VX=C.0
   VR=C.0

```



```

CALL VELCCY(VX,VR,BB,XB,4.712389)
IF(ABS(VX).LT..CCC001) GO TO 1CC
AGB=(XB-XCL(J))/(LMD*BB)
SRTB=SCRT(AGB*AGB-1.0)
XNUM=ST(J+1)*(1.0+VX)-VR
CENCM=LMD*SRTB+ST(J+1)*ALCG(AGB+SRTB)
ACL1(J)=XNUM/CENCM
ACL2(J)=ACL1(J)
WRITE(6,67) XH, RM, XFH, XX, TT, AM1(J), XB, BP, ACL1(J)
67 FCRMAT(2X,9F14.5)
1CC CCNTINUE
14 GNN=FLCAT(NCP)
CX=L3/GNN
X(1)=CX
CC 6 J=2,NCP
X(J)=X(J-1)+CX
6 CCNTINUE
CALL GECME(R,X,S,NCP)
WRITE(6,21)
WRITE(6,22)(X(J),R(J),S(J),J=1,NCP)
IF(IPLCT.EQ.0) GO TO 105
C*****
CALL GSIZE(8.0,11.0,11C0)
CALL PLCT(2.5,7.0,-3)
C*****
105 KS=C
THAC=THAC-45.0
CC 16 J=1,NPLOT
THAC = THAC+45.0
WRITE(6,8) THAC
8 FCRMAT(20X,7H THETA =F10.2)
THA=THAC/57.29578
CC 13 I=1,NCP
VX=C.0
VR=C.0
TT=R(I)
XX=X(I)
CALL VELCCY (VX,VR,TT,XX,THA)
BC=VR/(1.0+VX)
ERRCR=(BC-S(I))*57.29578
CP(I)=-2.0*VX+LMD*LMD*VX*VX -VR*VR
IF(CP(I).GT. 2.0) CP(I)= 2.0
IF(CP(I).LT.-2.0) CP(I)=-2.0
WRITE(6,29) I,VR,VX,BC,S(I),ERRCR,CP(I),X(I)
13 CCNTINUE
IF(IPLCT.EQ.0) GO TO 16
CC 17 I=1,NCP
CP(I)=CP(I)*10.0

```

```

17 CCNTINUE
  CC 12 I=1,15
  CPA(I)=CPA(I)*10.0
  CPE(I)=CPE(I)*10.0
18 CCNTINUE
  NCP1=NCP+1
  NCP2=NCP+2
  CP(NCP1)=0.0
  CP(NCP2)=1.0
  X(NCP1)=0.0
  X(NCP2)=1.0
  R(NCP1)=0.0
  R(NCP2)=1.0
  CALL FACTCR(.80)
  CALL AXIS(C.0,C.0,1,X,-1,6.0,C.C,X(NCP1),X(NCP2))
  CALL AXIS(C.0,-2.0,5HCPX1C,5,5.C,9C.0,-2.C,CP(NCP2))
  CALL SYMBCL(2.C,2.5,.10,2CHA4VIP-M=1.56-ALP=C.0,0.C,20)
  CALL SYMBCL(3.C,2.0,.10,14HEXPERIMENTAL--,0.0,14)
  CALL SYMBCL(999.0,2.05,.1C,C.C.C,0)
  CALL SYMBCL(3.C,1.7,.10,6THECRY,0.0,6)
  CALL LINE(X,CF,NCP,1,0,0)
  CALL PLOT(C.0,-4.0,-3)
  CALL AXIS(C.0,C.0,1,X,-1,6.C,C.C,X(NCP1),X(NCP2))
  CALL AXIS(C.C,C.0,1HR,1,1.C,9C.C,R(NCP1),R(NCP2))
  X(1)=C.0
  R(1)=C.0
  CALL LINE(X,R,N,1,0,0)
  CALL PLOT(6.0,C.0,2)
  CC 129 IK=1,N
  R(IK)=-R(IK)
129 CCNTINUE
  CALL PLOT(C.0,C.0,3)
  CALL LINE(X,R,N,1,0,0)
  CALL PLCT(6.0,C.0,2)
  CALL PLCT(C.C,C.C,999)
16 CCNTINUE
  STCP
  ENC

```

```

SUBROUTINE GEOMB(RAC,X,SLOPE,NS)
REAL L1,L2,L3,M117
DIMENSION RAD(NS),X(NS),SLOPE(NS)
COMMON/B/L1,L2,L3,RMAX,TAN2,A4VIP,M117,YTL
DO 999 I= 1,NS
  IF(X(I).GT.L1) GO TO 1000
C   NCSE SECTION
  YC=(L1**2-RMAX**2)/(2.0*RMAX)
  RAD(I)=-YC+SQRT((L1**2+YC**2)-(L1-X(I))**2)
  SLOPE(I)=(L1-X(I))/SQRT((L1**2+YC**2)-(L1-X(I))**2)
  GO TO 999
C   MIC-SECTION
1000 IF(X(I).GT.L2) GO TO 2000
  RAD(I)=RMAX
  SLOPE(I)=0.0
  GO TO 999
C   TAIL SECTION
2000 IF(X(I).GT.L3) GO TO 888
  RAD(I)=(-YTL+SQRT(((7.17860-L2)**2+YTL**2)-(X(I)-L2)**2))*
    *A4VIP+ (RMAX-TAN2*(X(I)-L2))*M117
  SLOPE(I)=(-(X(I)-L2)/SQRT(((7.17860-L2)**2+YTL**2)-(X(I)-
    *L2)**2))*A4VIP - (TAN2*M117)
  GO TO 999
888 RAD(I)=0.0
  SLOPE(I)=0.0
999 CONTINUE
RETURN
END

```



```

SUBROUTINE RHP(K,X,R,XI,RI,THA,ACC)
REAL LMC,KN
COMMON/AA/N,LMC,CLD
DIMENSION XI(N),RI(N)
C 41 FORMAT(1X,3F12.4)
C THIS SUBROUTINE DETERMINES HOW MANY OF THE SINGULARITIES
C IN BODY 1 OR 2 INFLUENCE THE CONTROL POINT X(J), R(J) ON
C BODY 1. THIS NUMBER IS STORED OR TRANSFERRED AS K.
Y = -R*COS(THA)
Z = R*SIN(THA)
DO 14 JJ=1,N
IF(XI(JJ).GT.X)GC TC 18
HPP=(X-XI(JJ))**2-LPD*LMC*((O.C-Y)**2+(RI(JJ)-Z)**2)-ACC
IF(HPP.LT.C.O) GC TC 18
K=K+1
14 CONTINUE
C 15 WRITE(6,41) K
18 RETURN
END

```

```

SUBROUTINE VELCT(K,X,R,XC,RO,AM,VX,VR,THA)
REAL LMD
COMMON/AA/N,LMD,CLD
DIMENSION XC(N),RO(N),AM(N)
IF(K.EQ.0) GO TO 18
DO 16 J=1,K
  CUMY = RO(J)*RO(J)+R*R
  RP = SQRT(CUMY-2.0*R*RO(J)*SIN(THA))
  AG = (X-XC(J))/(LMD*RP)
  SRT=SQRT(AG*AG-1.0)
  VX=VX-AM(J)*ALCG(AG+SRT)
  VRP= AM(J)*LMD*SRT
  SINB=R*CCS(THA)/RP
  CCSE=(RO(J)-R*SIN(THA))/RP
  VZ=-VRP*CCSE
  VY=-VRP*SINB
  VR=VR+VZ*SIN(THA)-VY*COS(THA)
16 CONTINUE
18 RETURN
END

```

```

SUBROUTINE VEL1(K,X,R,SI,A,VX,VR,THA)
REAL LMC
COMMON/AA/N,LMC,CLD
DIMENSION SI(N),A(N)
IF(K.EQ.0) GO TO 17
DO 16 J=1,K
  AG= (X-SI(J))/(LMC*R)
  SRT=SCRT(AG*AG-1.0)
  VX=VX-A(J)*ALCG(AG+SRT)
  VR=VR+A(J)*LMC*SRT
16 CONTINUE
17 RETURN
END

```



```

SUBROUTINE VELIT(K,X,R,SI,A,VX,VR,THA)
REAL LMC
COMMON/AA/A,LMC,CLC
DIMENSION SI(N),A(N)
IF(K.EQ.0) GO TO 17
VRP=0.0
DUMY=CLC*CLC+R*R
RP=SQRT(DUMY-2.0*R*CLC*SIN(THA))
CC 16 J=1,K
AG= (X-SI(J))/(LMC*RP)
SRT=SQRT(AG*AG-1.0)
VX=VX-A(J)*ALCG(AG+SRT)
VRP=VRP+A(J)*LMC*SRT
16 CONTINUE
SINP=R*CCS(THA)/RP
CCSE=(CLC-R*SIN(THA))/RP
VZ=-VRP*CCSE
VY=-VRP*SINE
VR=VR+VZ*SIN(THA)-VY*CCS(THA)
17 RETURN
END

```

```

SUBROUTINE VELCCY (VX,VR,TT,XX,THA)
COMMON/CC/SI(C60),A(C60),RCL2(C60),XIS(C60),RIS1(C60),
*AM2(C60),XCL(C60),ACL2(C60),AP1(C60),RCL1(C60),ACL1(C60),
*RIS2(C60)
C  MUST FIRST DETERMINE HOW MANY LINE SOURCE SEGMENTS INFLUENCE
C  CHECK INDUCED VELOCITIES FROM LINE SOURCES IN BODY 2. WE
C  THE CONTROL POINT J
K1 = 0
CALL R-P (K1, XX, TT, SI, RCL2, THA, .CCCCC1)
CALL VELCT(K1, XX, TT, SI, A, VX, VR, THA)
C  WE MUST NOW DETERMINE HOW MANY LINE SOURCES ALONG THE
C  IMAGE LINE OF BODY 2 INFLUENCE THE CONTROL POINT X(J), R(J)
C  NOW UNDER CONSIDERATION.
K2 = 0
CALL R-P (K2, XX, TT, XIS, RIS2, THA, .CCCCC1)
C  WE MUST NOW DETERMINE THE INDUCED VELOCITIES FROM THE LINE
C  SOURCE ALONG THE IMAGE LINE IN BODY 2.
CALL VELCT(K2, XX, TT, XIS, RIS2, AM2, VX, VR, THA)
C  WE MUST NOW DETERMINE HOW MANY LINE SOURCES ALONG THE
C  CENTERLINE OF BODY 2 INFLUENCE THE CONTROL POINT X(J), R(J).
K3 = 0
CALL R-P (K3, XX, TT, XCL, RCL2, THA, .CCCCC1)
C  WE MUST NOW DETERMINE THE INDUCED VELOCITIES FROM LINE
C  SOURCES ALONG THE CENTERLINE OF BODY 2.
CALL VELCT(K3, XX, TT, XCL, RCL2, ACL2, VX, VR, THA)
C  WE MUST NOW DETERMINE THE INDUCED VELOCITIES AT THE CONTROL
C  POINT DUE THE DISTRIBUTED SOURCES IN BODY 1 .
K4 = 0
CALL R-P (K4, XX, TT, SI, RCL1, THA, .CCCCC1)
CALL VELCT(K4, XX, TT, SI, A, VX, VR, THA)
C  WE MUST NOW DETERMINE THE INDUCED VELOCITIES AT THE SAME
C  CONTROL POINT FROM THE IMAGE LINE AND CENTERLINE LINE
C  SOURCES IN BODY 1.
K5 = 0
CALL R-P (K5, XX, TT, XCL, RCL1, THA, .CCCCC1)
CALL VELCT(K5, XX, TT, XCL, RCL1, ACL1, VX, VR, THA)
RETURN
END

```

467 CARDS READ

# INITIAL DISTRIBUTION

Hq USAF/RDQRM	2 TACTEC	1
Hq USAF/SAMI	1 USAFTAWC/TEFA	1
Hq USAF/XOXFM	1 TAWC/TRADOCLO	1
AFIS/INTA	1 ADTC/SES	1
AFSC/DLCA	1 ADTC/SD23	1
AFSC/IGFG	1 AFATL/DL	1
AFSC/SDZA	1 AFATL/DLOSL	2
AFAL/DHO	1 AFATL/DLY	1
AFWAL/Tech Lib	1 AFATL/DLJ	1
ASD/ENFEA	1 AFATL/DLJC	3
FTD/PDXA-2	1 AFATL/DLJF	1
AFML/LTM	1 AFATL/DLJK	1
AFWL/NSC	1 AFATL/DLJM	1
AFWL/NSE	1 USAF/XOOE	1
AFWL/SUL	1 USAFE/LGWM	1
AFEWC/SUR	4 AFSC/SDTA	1
AUL (AUL/LSE-70-239)	2 AFIT/LD	1
DDC	2 ASD/ENESS	1
NRSLC/MMIRBD	1 Naval Ship R&D Center/Code 166	1
Ogden ALC/MMWM	2 Naval Wpns Eval Fac	1
SAC/LGW	1 Comdr/USNWC/Code 4063)	1
SAC/NRI	1 AFATL/LDJA	1
TAC/DRA	1 AFFDL/FGC	1
57 FWW/DOS		
USAFTFWC/TA		
6510 ABG/SSD		
HQUSAFE/DOA		
HQUSAFE/DOQ		
HQPACAF/LGWSE		
HQPACAF/DOO		
Comdr/SARRI-LW		
Picatinny Ars/SARPA-TS-S#59		
Army Material Sys Analysis Agcy/ DRXSY-J		1
Army Material Sys Analy Agcy/ DRXSY-A		1
Redstone Sci Info Ctr/Chief, Doc Sec		2
USAE Waterways Experiment Stn/WESFE		1
Naval Rsch Lab/Code 2627		1
Navair Sys Comd		1
Navair Sys Comd/Tech Lib/AIR-954		1
Naval Surface Wpn Ctr/Tech Lib		2
Naval Ord Stn/Tech Lib		1
Nav Air Test Ctr/Tech Pubs		2
USNWC/Code 533		1
Sandia Lab/Tech Lib Div 3141		1
Rand Corp/Library-D		1